

Inhibition of MMP-2 Increases the Biomechanics of Fibroblast Tissue Rings

By

Yanying Wu

B.S., UC Davis, 2020

Thesis

Submitted in partial fulfillment of the requirements for the Degree of Master of Science in the Graduate Program of Biotechnology at Brown University

PROVIDENCE, RHODE ISLAND

MAY 2022

AUTHORIZATION TO LEND AND REPRODUCE THE THESIS

As the sole author of this thesis, I authorize Brown University to lend it to other institutions for the purpose of scholarly research.

Date 2022-04-01



Yanying Wu, Author


I further authorize Brown University to reproduce this thesis by photocopying or other means, in total or in part, at the request of other institutions or individuals for the purpose of scholarly research.

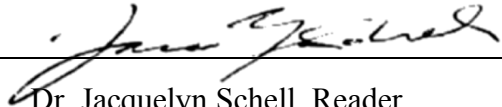
Date 2022-04-01




Yanying Wu, Author

This thesis by (Yanying Wu) is accepted in its present form by the Graduate Program in Biotechnology as satisfying the thesis requirements for the degree of Master of Science

Date 4/18/22 Signature: 
Dr. Jeffrey Morgan, Advisor

Date 4/18/22 Signature: 
Dr. Jacquelyn Schell, Reader

Date 4/19/2022 Signature: 
Dr. Toni-Marie Achilli, Reader

Approved by the Graduate Council

Date _____ Signature: _____
Dr. Andrew G. Campbell, Dean of the Graduate School

Acknowledgments

I would like to thank all the people at Brown University for providing me with an incredible master's experience. I sincerely express my most profound appreciation to my advisor, Dr. Jeffrey Morgan, for being an excellent mentor who welcomed me to the lab and provided me with personal and professional support all the time. I would like to thank Caitlin Hopkins for coaching me through many challenging technical skills and giving valuable feedback through my experiments and my thesis; Blanche Ip, Karl Anderson, and Joshua Manning for helping me to solve important tasks. I would like to thank every individual in Morgan Lab for always being available to me when I encountered difficulties and for providing a supportive and collaborative culture. Also, I would like to thank Dr. Jacquelyn Schell for being a supportive and understanding program director during my study at Brown. Finally, I would like to acknowledge my family and friends for their love and encouragement as I pursue my master's study.

Table of Contents

Signature Page.....	ii
Acknowledgments.....	iv
Abstract.....	1
Introduction.....	2
Matrix metalloproteinases (MMPs) superfamily.....	2
Matrix metalloproteinases (MMP) -2.....	5
Incyclinide an inhibitor of MMP-2.....	7
3D <i>in vitro</i> fibroblast ring-shaped microtissue model.....	9
The Importance of Biomechanics in ECM.....	10
Materials and Methods	13
Cells and culture conditions.	13
Fabrication of the mold used to make ring-shaped tissues.	14
Mechanical testing of ring-shaped tissues.	15
Data analysis and visualization.	16
Statistical analysis.	17
Results	18
The morphology of the 3D rings changes in the highest dose of incyclinide.....	18
Tissue ring thickness decreases over time in an incyclinide dose-dependent manner.....	21
The dermal fibroblast rings migrate at different distances around the peg	24
Low doses of incyclinide do not affect the cross-sectional area or volume of rings.....	26
Inhibition of MMP-2 increases the biomechanical properties of fibroblast tissue rings	28
Discussion and Conclusion.....	35
References	42

Table of Figures

Figure 1: The category of MMPs.	3
Figure 2: The process of MMP activation in the extracellular medium environment.....	4
Figure 3: The Scheme figure of the activation of MMP-2 on the cell surface.....	6
Figure 4: A typical stress-strain curve represents the object's mechanical properties.....	11
Figure 5: Formation of tissue rings using stainless steel molds.	18
Figure 6: The bright-field images of 3D microtissue rings over times	19
Figure 7: The morphological change of the rings over time.....	20
Figure 8: The change of thickness in 3D microtissues over time.....	23
Figure 9: The migrated distances of the rings.....	25
Figure 10: The cross-sectional area and the volume of the rings	27
Figure 11: The tensile strength of rings	33
Figure 12: The stiffness of the rings	34
Figure 13: The schematics figure of the interaction of TGF- β and MMPs.....	37

Table of Tables

Table 1: Three major pathologies caused by MMPs.....	5
--	---

Abstract

Synthesis and degradation of the extracellular matrix (ECM) are important for tissue development, morphogenesis, repair, and remodeling. Multiple proteinases are involved in the degradation of ECM, but matrix metalloproteinases (MMPs) are the most important ones, especially with regards to collagen which is resistant to proteolytic digestion. Inhibitors of MMPs have been proposed as emerging targets in the treatment of cancer, fibrosis, and cardiovascular diseases. Dermal fibroblasts produce MMP-2 and incyclinide, an inhibitor of MMP-2, has been extensively investigated and even evaluated in several clinical trials, but with disappointing results. To aid in the development of new drugs that can influence the ECM, there is a need for new *in vitro* models that can replicate the 3D architecture of the human ECM and its biomechanics. In this research, a 3D *in vitro* fibroblast microtissue ring model was tested. This model creates a highly aligned human ECM environment that mimics the histological and mechanical properties of ligamentous tissues. Different doses of incyclinide were tested on the fibroblast rings to test its effects on MMP-2. By measuring the morphological change, the ultimate tensile strength (UTS), and the maximum tangent modulus (MTM) of the rings, we found that the biomechanics of tissue rings treated with 5 μ M incyclinide increased significantly. This indicated that inhibition of MMP-2 influenced the collagen and proteins in the ECM in a way that increased biomechanics. Besides the inhibitory effect of MMP-2, incyclinide also showed toxic effects at the highest dose, including the inhibition of cell growth and proliferation, as well as the apoptosis of cells. These results provide valuable insights into a new 3D model for testing new treatments that target the complex proteins of the extracellular matrix.

Introduction

Matrix metalloproteinase (MMPs) superfamily

The extracellular matrix (ECM), composed of a sophisticated network of biomacromolecules, plays vital roles in supporting structural and biochemical functions in all organs and tissues. Based on differences in cell types, their growth environment and functions, ECM is developed with tissue specificity, which is manifested as the diversity of components, including fibers, proteoglycans, growth factors, glycoproteins, and polysaccharides. The abundance of collagen and elastin in ECM determines the mechanical properties to a major extent, such as structural integrity, stiffness, and tensile strength. The structure of the ECM is dynamic and requires constant remodeling to regulate homeostasis [1]. Therefore, degradation of the ECM is important for tissue development, morphogenesis, and remodeling and even has a significant impact on the cellular phenotype. Various proteinases take participations in the process of ECM degradation, among which Matrix metalloproteinases (MMPs) are the most important enzymes in this course [2].

The MMPs are composed of various proteolytic enzymes with a zinc-dependent active site [2]. The main function of MMPs is to facilitate cells or tissues to degrade multiple components, including extracellular matrix proteins, glycoproteins, growth factors, membrane receptors, and cytokines [5]. The MMPs play an important part in multiple physiological processes, including remodulation of tissue, healing of wounds, cell differentiation, cell proliferation, morphogenesis, cell apoptosis, etc. There are twenty-eight types of MMPs among vertebrates and twenty-three MMPs are presented in human tissue. MMPs contain similar structures, but little variation among different types. Each MMP possesses a signal N-terminal peptide that directs secretion of the also

enzyme; a pro-domain part that regulates the enzyme with inactive status; and a domain with catalytic functions that contain zinc. Most MMPs also have a hemopexin-like structure domain and a biolinker that connects the catalytic domain with the hemopexin-like domain. Because of their substrate specificity, the construction of the domain, and the similarity of sequences, the MMPs can be categorized into the following groups: collagenases, gelatinases, stromelysin, matrilysin, membrane-type metalloproteinases, as well as others (**Figure 1**).

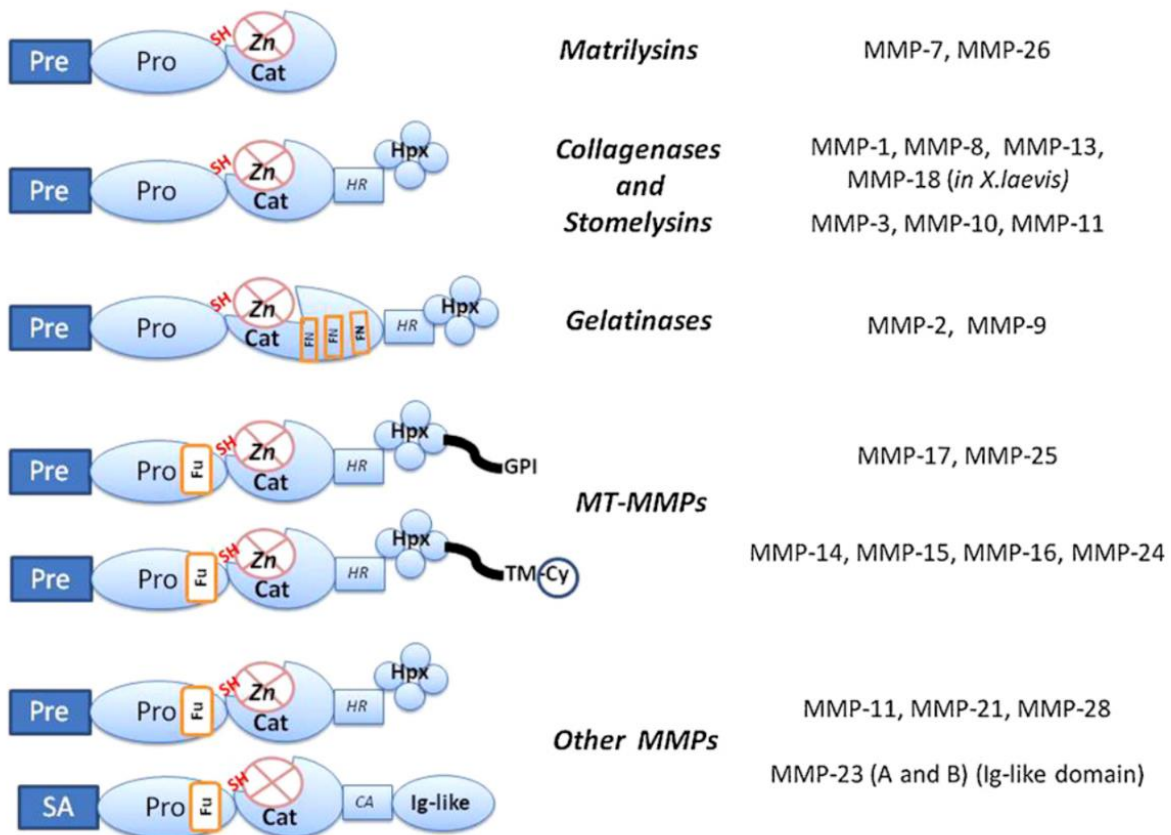


Figure 1: The category of MMPs. MMPs can be categorized into 6 groups according to the specificity of the substrate and the construction of their domains. Most of the MMPs are comprised of three principal regions: N-terminal signal sequence (Pre), a pro-domain (Pro) with one thiol group, as well as the catalytic domain with a site for zinc-binding (Zn^{2+}). The figure was adopted from Mannello et al. [6]

Activation of MMPs is tightly regulated. MMPs are produced by various cells (*e.g.*, pro-inflammatory cells) and tissues (*e.g.*, connective tissue), including vascular smooth muscle cells, fibroblasts, leukocytes, and macrophages [3,4]. Tissues and cells synthesize MMPs in the form of the zymogen, the inactive precursor without the signal peptide, which gets activated in the medium of the extracellular environment. The activation mechanism is a “stepwise activation”. Firstly, the proteolytic attacks on the “bait region”, and then each MMP dictates specified cleavage. The cleavage leads to the destabilization of the pro-domain. This process includes the interaction of the cysteine switch-zinc, which gives rise to the intramolecular processing and MMP activation (**Figure 2**) [2, 6]. Also, MMP expression is controlled by secretion, transcription, and inhibition by MMP inhibitors. Failure to control the expression or activity of MMPs might result in MMP deregulation, which results in three major groups of pathologies, including tissue destruction, fibrosis, and matrix weakening (**Table 1**) [2].

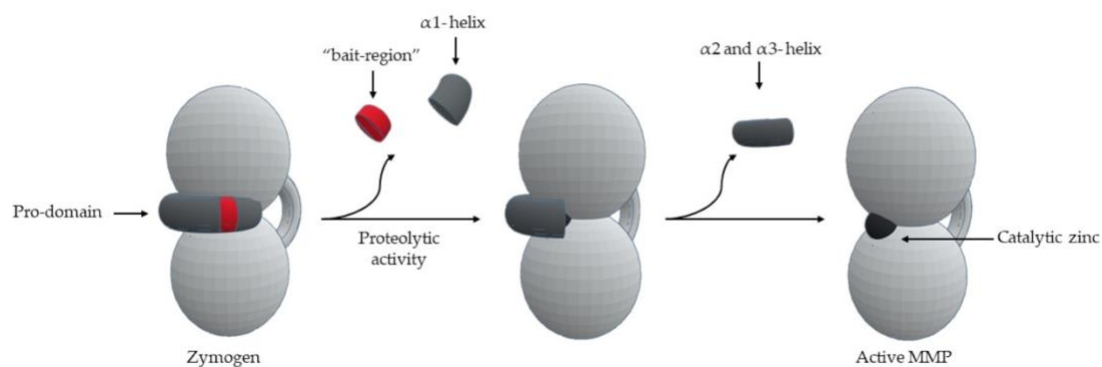


Figure 2: The process of MMP activation in the extracellular medium environment. The first step is the proteolytic attack on the bait region from the pro-domain of the zymogen. The process of the pro-domain removal makes the remaining pro-domain unstable, leading to activation of the catalytic zinc site. Figure reproduced from Laronha et al. [2]

Table 1. Examples of diseases caused by deregulation of MMPs.

Pathologies	Diseases
Tissue destruction	Cancer invasion and metastasis
	Arthritis
	Ulcers
	Periodontal diseases
	Brain degenerative diseases
Fibroses	Liver cirrhosis
	Fibrotic lung disease
	Otosclerosis
	Atherosclerosis
	Multiple sclerosis
Weakening of matrix	Dilated cardiomyopathy
	Aortic aneurysm
	Varicose veins

Table 1: Three major pathologies caused by MMPs. Due to the activation of MMPs, factors that can trigger diseases can be divided into (1) destruction of tissue, (2) fibrosis, and (3) matrix weakening. The figure was adopted from Laronha et al. [2]

Matrix metalloproteinase-2 (MMP -2)

MMP-2, a soluble protein, is regulated by the process of transcription, translation, secretion, zymogen activation (**Figure 2**), and regulation of its inhibitor [12]. Various tissues and cells, including dermal fibroblasts, produce MMP-2 [9,10]. In cells, after the process of transcription, translation, and secretion, the inactive MMP-2 (proMMP2) is produced and then located on the cell surface. Followed by this process, the enzyme activation is then modulated by binding with tissue inhibitor of metalloproteinase 2 (TIMP-2) and type-1 membrane MMP (MT1-MMP, or MMP-14) (**Figure 3**) [12, 13].

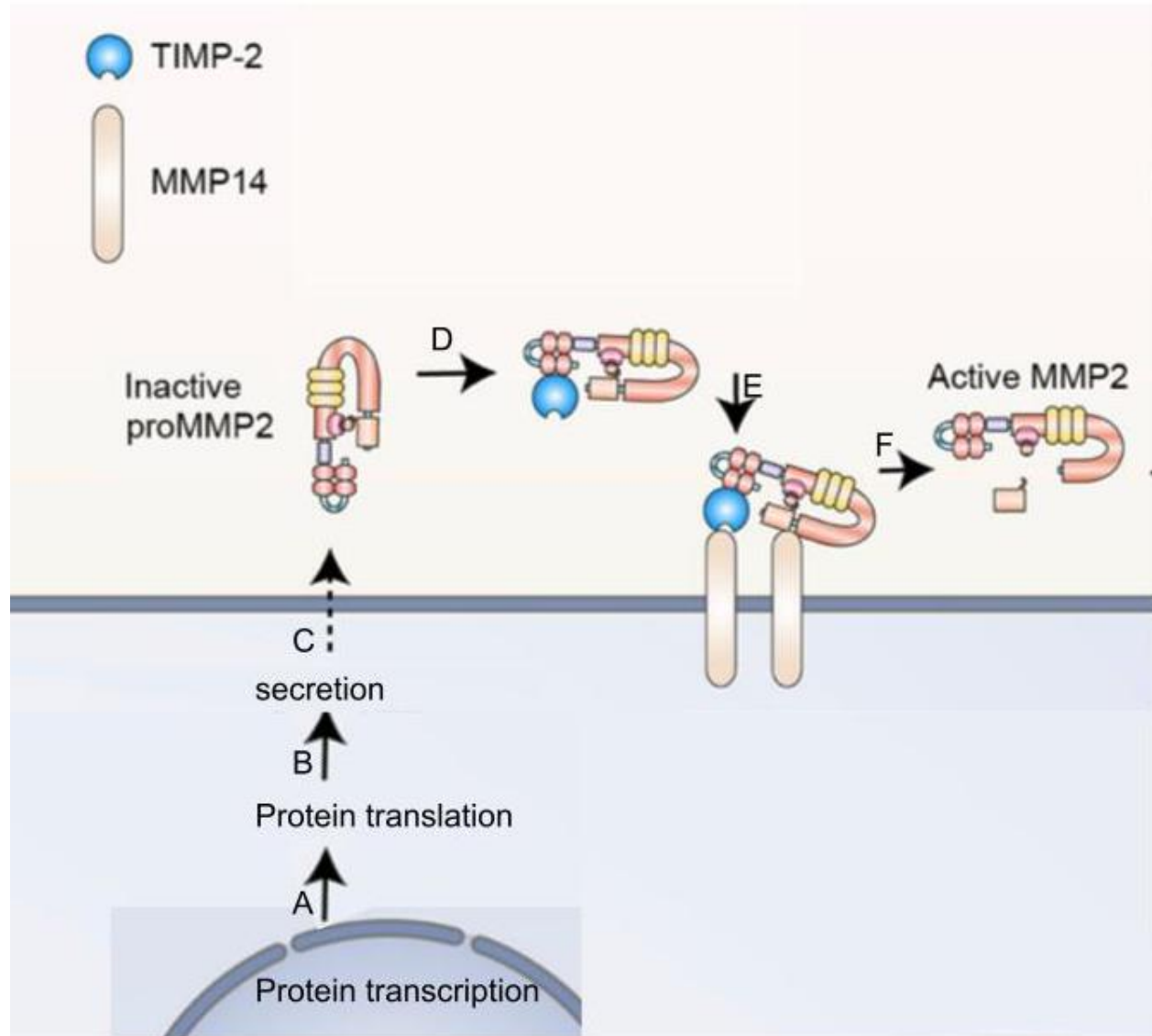


Figure 3: The Scheme figure of the activation of MMP-2 on the cell surface. After secretion by the cell, inactive proMMP2 is activated by the combination of TIMP-2 and MMP14. This proMMP2/TIMP-2/MMP14 complex then binds MMP14 on the cell membrane and transforms the proMMP2 into the activated form. The figure was reproduced from Li et al. [7].

MMP-2, the enzyme involved in breaking down type IV collagen, works as an important part of the basement membranes in ECM and performs multiple significant roles for tissue homeostasis, including the reconstruction of new blood vessels, the remodeling of bone, and the repair of organs [11]. However, the dysregulation of MMP-2 activity facilitates cancer invasion and metastasis, such as breast cancer, pulmonary cancer, esophageal cancer, and osteosarcoma [2,

12, 14]. In breast cancer, preventing the process of metastasis is important. The elevated level of MMP-2 affects the level of Twist1-induced migration and metastasis, and a decline in MMP-2 expression leads to the expression of a tumor suppressant, RNA binding protein 3 (RBMS3) [15]. In breast cancer cells, other molecules affect the expression of MMP-2; TGF- β 1, TIMPs as well as reversion-inducing cysteine-rich protein (RECK) regulate the expression of MMPs, including MMP-2 and MMP-9 [18], whereas TGF- α stimulates the activity of MMP-2 [18,19]. In lung cancer, the level of MMP-2 expression is also markedly increased and is related to the invasion and metastasis of tumors by different pathways, including the sphingolipid signaling pathway [12, 16]. Moreover, during the metastatic process, MMP-2 hyperactivation results in osteolytic lesions causing tumor migration to the bone [17]. In the tumor-bone environment, MMP-2 amplifies its effects by modulating the expression of different growth factors, for example, TGF- β [20]. The hyperactivity of TGF- β is closely related to cancer metastasis [21]. Besides cancer metastasis, the dysregulation of the expression of MMP-2 is also related to other diseases, such as inflammation, asthma, cardiovascular disease, and fibrosis [2].

The expression and function of MMP-2 are strictly controlled in physiological processes by endogenous protease inhibitors, for example, tissue inhibitors of metalloproteinases-2 (TIMP-2). MMP-2 can also be regulated by drugs, such as tetracyclines. Tetracyclines (TCs) are antibiotics that are well known for their anti-bacterial properties. Doxycycline (DC), the most widely TC derivative, is an affordable and safe drug for the prevention of various bacterial infections, such as sexually transmitted diseases and urinary tract infections [23]. Chemically modified tetracycline (CMT) was firstly demonstrated in 1987 [22], and later, TCs were proven to be inhibitors of MMPs through *in vivo* and *in vitro* experiments [23. 25]. The most notable characteristic of CMTs was the deletion of anti-bacterial properties, along with the enhancement

in the inhibition of MMPs [26]. Numerous research and clinical trials have been conducted on CMT-3, also known as incyclinide, as an effective inhibitor for MMP-2.

Incyclinide as an inhibitor of MMP-2

Incyclinide inhibits MMP-2 by interfering with the interaction between MMP-2 and MMP-14 (**Figure 3**) and as a result, the MMP-2 cannot be activated [24]. Incyclinide is proven to have an anti-tumor effect in both *in vitro* and *in vivo* experiments. *In vitro*, incyclinide has shown to have an inhibitory effect on MMP-2 and MMP-9. In prostate cancer cell lines, PC-3 and DU-145, incyclinide inhibited the cell growth with a GI₅₀ of 12 μM and diminished their invasiveness into Matrigel, a solubilized basement membrane, with an IC₅₀ of 3.77 – 5.39 μM [27]. *In vivo*, incyclinide has been reported to inhibit the metastases of the organic bone matrix and prostate tumor growth in the rat Dunning MAT LyLu prostate cancer model [28]. At 10 μM, the Dunning MAT LyLu prostate cancer line underwent cell apoptosis [27]. Von den Hoff *et al.* demonstrated that incyclinide inhibited the degradation of the organic bone matrix by preventing orthodontic tooth displacement in rats [29].

Based on the efficacy of incyclinide in preclinical research, incyclinide was also researched in multiple clinical trials. Incyclinide has been studied in one Phase II clinical trial for Kaposi sarcoma [31], a rare kind of cancer commonly developed in people with immune deficiencies, and recurrent brain tumors [32]. In the Phase II study of sarcoma, the clinical trial was terminated because, after a 50 mg/m² daily dose treatment in 8 weeks, most of the patients did not show response and even 33% of patients experienced tumor progression [34]. Another Phase I clinical trial was conducted on the effects of oral incyclinide on patients with refractory metastatic cancer [33]. Incyclinide was used orally in cancer patients on a continuous schedule. When administrated in maximum doses of up to 70 mg/m² every day, there were common side effects including

photosensitivity and fatigue [35]. Also, for incyclinide, the preliminary pharmacologic analysis demonstrated that at the maximum tolerable doses, the steady-state plasma concentrations surpassed the IC_{50} in the *in vitro* research [33, 35].

Since the 1990s, a lot of research has been done on testing MMP inhibitors as drug targets for tumor invasions and metastases. Among all the experiments mentioned above, animal models are needed to test out the efficiency and toxicity of incyclinide in preclinical trials. However, using animals' models can be costly and usually need the models to be modified on the genetics level which interferes with their ability to simulate the pathological environment of human diseases. Moreover, despite the powerful preclinical data, the clinical trials still face challenges such as some patients in clinical trials experienced serious side effects, while some experienced ineffectiveness after treatment. Some of these problems may be solved by creating more advanced *in vitro* models.

3D *in vitro* fibroblast ring-shaped microtissue model

An interesting and relevant 3D *in vitro* model was developed in the Morgan Lab at Brown University. The model produces a collagen-rich ECM environment that is highly aligned, and most importantly, mirrors the histological and mechanical properties of ligamentous tissues [37]. One of the innovative advantages of this model is the elimination of the need for prefabricated polymer scaffolds [37]. The existing *in vitro* models, mostly require the cells to be embedded in synthetic scaffolds [36], which creates significant crosstalk between cells and the scaffold and affects the cellular synthesis, collagen alignment, and tissue biomechanics. In the new model, human dermal fibroblasts are directly seeded in a ring-shaped mold, where the cells self-assemble around the central agarose peg and eventually formed a microtissue ring [37]. Another benefit is that this model enhances the biomimicry compared with the 2D and 3D models. This model successfully

replicates the most important biomechanical properties of ligaments and tendons [37]. In response to the radial tension generated by the ring-shaped mold, the cells are forced to create a protective matrix as their own ECM, against the stress in the same direction toward the peg.

Based on this model, Wilks *et.al.* demonstrated the role of formulation of the media and time needed for the cellular alignment development, synthesis of collagen, as well as mechanical properties. Eventually, the seeding density and media formulation of the mold were optimized and utilized in the following experiments. Transforming growth factor (TGF)- β 1 increased the biomechanics of the fibroblast rings in a dose-dependent manner [37].

The importance of ECM biomechanics

Research has demonstrated that biomechanics are of equal importance as biochemistry in cellular interaction [38]. In ECM, filamentous collagen-based structures such as tendons and ligaments, make up a complicated layered structure of collagen fibers that make up approximately 80% of the ECM. The rest 20% comes from cells grown beside the collagen fibers [39]. Several biomechanical properties are critical to our research.

Young's modulus is a physics term that demonstrates the elastic properties of a solid object when it takes tension or compression. It is a measurement of the ability of the object to resist changes in length [41]. In biomechanics, the young's modulus can be calculated using stress/strain data and works as an indicator for the stiffness of the tissue or ECM [40]. Stress and strain are terms to describe one object's ability to resist externally applied forces. Once the force is applied to the tissue or cellular matrix, the internal structure of the tissue or cellular matrix will change to resist that force. The internal force created inside the object that is meant to resist is termed stress, which is calculated by dividing the force by area and is in units of megapascals (MPa) [40]. The

deformation of the tissue as a result of the externally applied forces is termed strain. Stress and strain can be graphed together. This diagram is called a stress-strain curve. By reading the trend of the curve, one can retrieve useful information on the properties of materials. In the diagram, stress is placed on the y -axis and strain is on the x -axis. This curve (**Figure 4**) can reveal many properties of the material object, such as the ultimate tensile strength (UTS) and the maximum tangent modulus (MTM) [41].

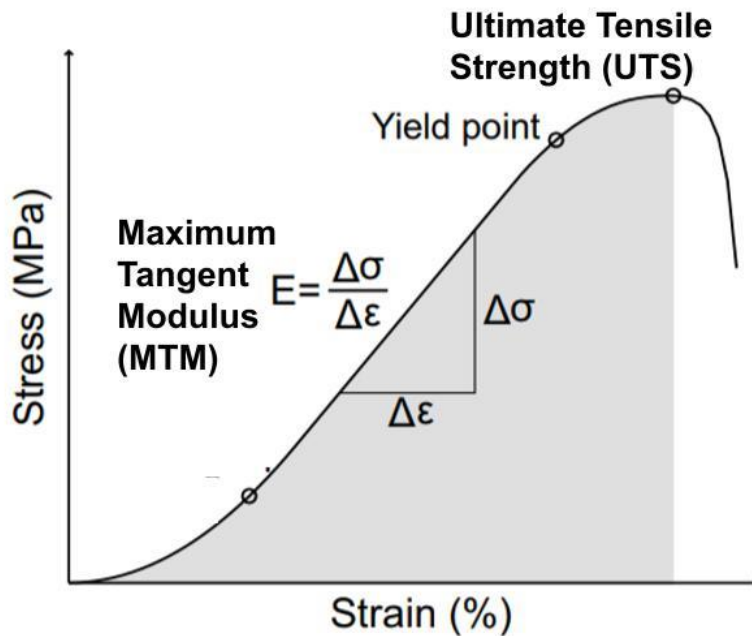


Figure 4: A typical stress-strain curve represents the object's mechanical properties. The stress is in the unit of MPa. With increased stress applied to the object, the object will undergo increments in deformation. The gradient before the maxima represents the maximum tangent modulus (MTM). The curve's maxima are called ultimate tensile strength, meaning the stress applied before breakage. The yield point indicates the limit of elastic behavior of the object. The figure has been reproduced from Ristaniemi et al. [40]

In this research, the major goal is to characterize the effects of different doses of incyclinide on the fibroblast microtissue rings as an MMP-2 inhibitor. MMP-2 is an important component in the process of breaking down the ECM, which is essential to tissue homeostasis, including the reconstruction of new blood vessels, the remodeling of bone, and the repair of organs. With the

inhibition of MMP-2, we anticipate that in our fibroblast tissue ring model, the biomechanics of rings treated with 1 μ M, 5 μ M, and 10 μ M should increase in a dose-dependent manner, meaning all the incyclinide-treated rings should have stronger mechanical properties, compared with the vehicle control rings. Moreover, there might be other effects worth consideration, such as growth inhibition of the drug on the rings. For this research, we found that by comparing to the control group, the biomechanics of the 1 μ M incyclinide-treated group showed no significant difference, but the biomechanics of the 5 μ M incyclinide-treated group increased significantly on day 14. However, as the concentration of incyclinide reached 10 μ M, the biomechanics decreased compared to the control rings. The results mostly matched our expectations. The increase of biomechanics at 5 μ M in the incyclinide-treated rings indicated that the inhibition of MMP-2 led to the increase of collagen and proteins in ECM. The decrease of biomechanics in the 10 μ M incyclinide-treated group indicated the toxicity effect triggered by this concentration. However, the effects of incyclinide on the collagen arrangement and the types of collagen contents in ECM need further validation. These results could provide valuable insights into the treatment of diseases with extracellular matrix degradation of collagen modification.

Materials and Methods

Cells and culture conditions.

Juvenile normal human dermal fibroblasts (jNHDF) were acquired from PromoCell, Heidelberg, Germany. jNHDFs were cultivated in a pre-made cell culture medium. The medium was composed of high glucose, L-glutamine, phenol red, and sodium pyruvate DMEM (Dulbecco's Modified Eagle's medium) (119995065, Thermo Fisher Scientific, Waltham, MA) with 10 % fetal bovine serum (FBS) (GIBCO) and 1 % penicillin/streptomycin. They were kept in the incubator at 37 °C and 10% CO₂. Using a standard trypsin protocol, jNHDFs were passaged from P5 to P9. After rinsing using phosphate-buffered saline (PBS) (SH30256.FS, Thomas Scientific, Swedesboro, NJ), jNHDFs were trypsinized at 0.05% concentration in PBS for 5 minutes. Following this, the culture medium with FBS was added to stop the trypsinization. The cells were centrifuged at 800 RPM for 6 min. Then, they went through the process of resuspension and cell counting. Finally, cells were plated in a T-175 flask (Corning, NY) with a density of 4.3 – 7.0 x10³ cells/cm².

3D microtissue rings were cultivated in a 50:50 combined medium. 50:50 medium was composed of a mixture of serum-free medium plus (SFM+) and serum-free medium advanced (SFMA). The SFM+ was composed of the serum-free DMEM with 0.1 mM 2-phospho-l-ascorbic acid trisodium salt (Sigma- Aldrich, St. Louis, MO), 50.0 µg/ mL l-proline (Thermo Fisher), 1% penicillin/streptomycin. The SFMA was the advanced DMEM (12491015) supplemented with 1% penicillin/streptomycin. For the construction of 3D microtissue rings, 300,000 jNHDF cells were seeded into a well with 75 µL of 50:50 medium and allowed to settle for 45 – 60 min, before 1 ml

of 50:50 media was slowly pipetted into each well. Medium changes were performed on Days 1, 2, 5, 7, 10, and 12.

Fabrication of the mold used to make ring-shaped tissues.

Benjamin T. Wilks designed the molding system using CAD software (SolidWorks Corporation, Concord, MA). The gel-molding system was divided into two major parts: 24 ring-shaped molds and a holder [37]. The ring-shaped molds were constructed from stainless steel 316L (Protolabs, Maple Plain, MN) and each mold was designed to be fitted into one well of a standard 24-well plate. The holder was designed to sit over the top of a standard 24-well plate and was fabricated from aluminum. The holder contained 24 holes, each hole over the top of one well of the 24-well plate. After adding 1.5 mL of 2% molten (w/v) agarose (BP160-500, Fisher Scientific, Hampton, NH) in PBS to each well of the 24-well plate, the aluminum holder with the stainless-steel inserts was placed on the top of the plate for 15 min. After the removal of the molds, each well contained a molded agarose gel with an inner 5-mm diameter and a 0.75-mm surrounding a cylindrical trough. Gels were equilibrated in SFM with 1 % penicillin/streptomycin at 10 % CO₂ and 37 °C. After three medium changes, the gels were ready for use.

Incyclinide treatment of ring-shaped tissues.

After 24 hours of the seeding process, different doses of incyclinide were added to the system. 10 mg of Incyclinide (MedChemExpress, Monmouth Junction, NJ) were dissolved in 2.693 mL dimethyl sulfoxide (DMSO). The incyclinide with a final concentration of 10 mM was separated into aliquots of 45 µL and stored at -80 °C. On Day 1, 2, 5, 7, 10, and 12, ring-shaped tissues were fed with the mixing of the different doses of incyclinide and DMSO from the frozen

aliquots and the 50:50 SFM+/SFMA medium. On day 1, because of the equilibration of 1.5 mL gel, the dosage amount was added in a 2.5-time manner. Therefore, on day 1, the incyclinide was reconstituted in DMSO and resuspended in final concentrations of 25, 12.0, 2.5, and 0 μM medium for feeding the rings., 10.0, 5.0 1.0, and 0 μM of the incyclinide medium was used on day 2, 5, 7, 10, and 12. To prepare the highest concentration of inhibitory media, 20 μL of the aliquot was mixed with 20 mL of 50:50 media to archive a final concentration of 10 μM incyclinide. To make the 5 μM incyclinide-treated media, 10 μL of the aliquot and 10 μL of DMSO were thawed in 20 mL of 50:50 medium. To formulate the 1 μM incyclinide-treated media, 2 μL of the aliquot and 18 μL DMSO were thawed in 20 mL of 50:50 SFM+/SFMA medium. The vehicle control was a mixture of 20 μL DMSO and 20 mL 50:50 media.

Mechanical testing of ring-shaped tissues.

Mechanical testing of fibroblast ring-shaped tissues was performed on an Instron tensile tester (5943, Norwood, MA) using a 5N load cell with 5 mN resolution. Each gel was removed from the plate by a spatula and cut on one side with a razor blade to obtain side-view images of the ring-shaped tissue. The top-view and side-view brightfield images were taken at 2x magnification on a Nikon Eclipse Ts2 microscope (Nikon, Tokyo, Japan). Thickness measurements of the tissue from these images were used to calculate the cross-section area (A_0) of the ring-shaped tissue. Before mechanical testing, rings were removed from the gel and were placed over two custom 3D printed grippers made from glass-filled nylon (PA614-GS, ProtoLabs). Each gripper was one-half of a cylinder with a 1.5mm-radius. The initial distance between grippers was extended by 2 mm to reach a diameter of 5 mm. As a result, the quasistatic loading was achieved. During the test, an automatic termination occurred when the load dropped below 40%,

indicating tissue failure. A BlackflyS, Color Camera (BFS-U3-200S6C- C USB3, Edmund Optics, Barrington, NJ) was equipped to record the images during mechanical testing.

Data analysis and visualization.

The mechanical data analysis protocol and software were adapted from Wilk et.al. [37] Using Python 3.6 (Python Software Foundation) and the package of statistical models, SciPy, Matplotlib, NumPy, Pandas, scikit-image, and scikit-posthocs, mechanical properties were quantified [37]. Data from raw load measurements were normalized to eliminate the drag force. The drag force was obtained by performing mechanical testing under the same conditions and the same equipment without rings on the grippers. The mechanical testing protocol was based on Gwyther *et. al.* and Adebayo *et. al.* and was improved by Wild *et. al.* [41, 37] When the raw load exceeded 5mN, the extension length, and the raw load was recorded since the tissue was assumed to be under tension.

To determine the essential biomechanical properties of the tissue, the maximum tangent modulus (MTM), the ultimate tensile strength (UTS), and the failure strain were calculated using the engineering stress ($N/2A_0$) and the engineering strain ($\Delta L/L_{gauge}$). In this equation, A_0 indicates the elliptical cross-sectional area. The slope of the stress-strain curve represents the tangent modulus, which can be obtained by fitting the curve over a region of 8% strain for all the points [37, 39]. All procedures followed the previous literature which demonstrated the maximum tangent of the modulus, the young's modulus, and stiffness. In our tests, the maximum tangent modulus (MTM) was within the linear range of the stress-strain curve. However, the engineering stress and strain are measurements only applicable for minor deformations and are not suitable for measuring many biological samples [39, 40]. True stress and strain were also limited because they are

accurate only under the same assumption [37, 39]. All the mechanical test results, including engineering stress-strain, the true stress-strain, as well as calculations using minimum and mean cross-sectional area are described in the Results section.

$$\text{Engineering Strain} = \Delta L / L_{\text{gauge}} \quad (1) [37]$$

$$\text{Engineering Stress} = N / (2A_0) \quad (2) [37]$$

$$\text{True Strain} = \ln(1 + \text{Engineering Strain}) \quad (3) [37]$$

$$\text{True Stress} = \text{Engineering Stress}(1 + \text{Engineering Strain}) \quad (4) [37]$$

Statistical analysis.

All mechanical data was plotted in the form of box plot graphs. Each point on the graph represents a sample. The horizontal lines and the vertical lines represent the mean \pm standard error. All graph and statistical analysis were done in PRISM 9.0.0 (GraphPad Software, San Diego, California USA, www.graphpad.com). To test the normal distribution, normality was tested with Shapiro–Wilk test, Kolmogorov-Smirnov tests, and D'Agostino & Pearson tests, respectively. To calculate the statistical significance among multiple groups, ordinary two-way ANOVA with main effects only and Tukey's multiple comparisons test with individual variances were computed for each comparison. In the graphs, the unique labeled letter * showed the statistical significance ($p < 0.05$) between experimental groups.

Result

The morphology of the 3D rings changes in the highest dose of incyclinide

The stainless-steel molds, which enable the fabrication of microtissue rings, were previously developed by our former members (**Figure 5**) [49]. The molding system is composed of two parts: 24 small stainless-steel inserts, where each inset has a 5-mm diameter ring that is 0.75-mm thick, and a stainless-steel holder, which matches perfectly with a standard 24-wells plate. To produce circular troughs each with a 5-mm diameter central peg, the stainless-steel inserts were inserted into wells containing 2% liquid agarose for gel formation (**Figure 5B**). After 15 minutes, the insets were removed, and the agarose molds were formed within a 24 well plate. 300,000 Juvenile normal human dermal fibroblasts (jNHDF) cells were then seeded into each well for fabrication to develop their own ECM environment in 50:50 media (**Figure 5C**). 50:50 media was used for seeding and feeding over 14 days, and it was a mixture of SFM+ and SFMA. The cells self-assembled around the 5-mm central agarose peg and eventually formed a microtissue ring (**Figure 5D**).

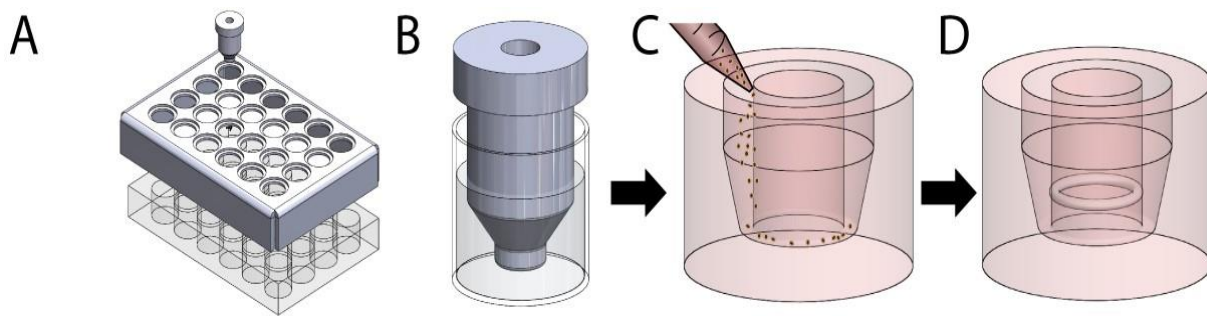


Figure 5: Formation of tissue rings using stainless steel molds. The stainless-steel molds, which enable the fabrication of the microtissue rings, were previously developed. (A). The scheme figure of the two-part mold. (B). Stainless steel was embedded in wells with 2% liquid agarose gel to produce troughs with the 5-mm diameter central peg. (C&D). 3×10^5 Juvenile normal human dermal fibroblasts (jNHDF) cells were seeded into each well to self-assemble and form a ring-shaped microtissue in 50:50 media.

Incyclinide is an inhibitor of MMP-2 and MMP-14. To investigate the effects of incyclinide, the drug (10 μ M, 5 μ M, 1 μ M) and vehicle control were added 24 hours after the cells were seeded. According to Lokeshwar et al. [50], when CaP139 cells, a cell type with prostate cancer, were treated with incyclinide, MMP-2 level decreased by 56.7 % and 74.0 % respectively with a dose of 5 μ M and 10 μ M. The exact amount of DMSO (10 μ M) in the vehicle control group was also added. In the 5 μ M and 1 μ M incyclinide-treated groups, an extra amount of DMSO (5 μ M and 9 μ M) was added to control for the DMSO's effects on the rings. jNHDF were seeded on three 24-well plates on day 0 for each independent experiment, and each group had at least 15 rings on day 1. Two bright-field images of the top view of each ring were taken at 2x magnification on Days 1, 4, 7, 10, and 14 and were stitched together using Fiji software (**Figure 6**).

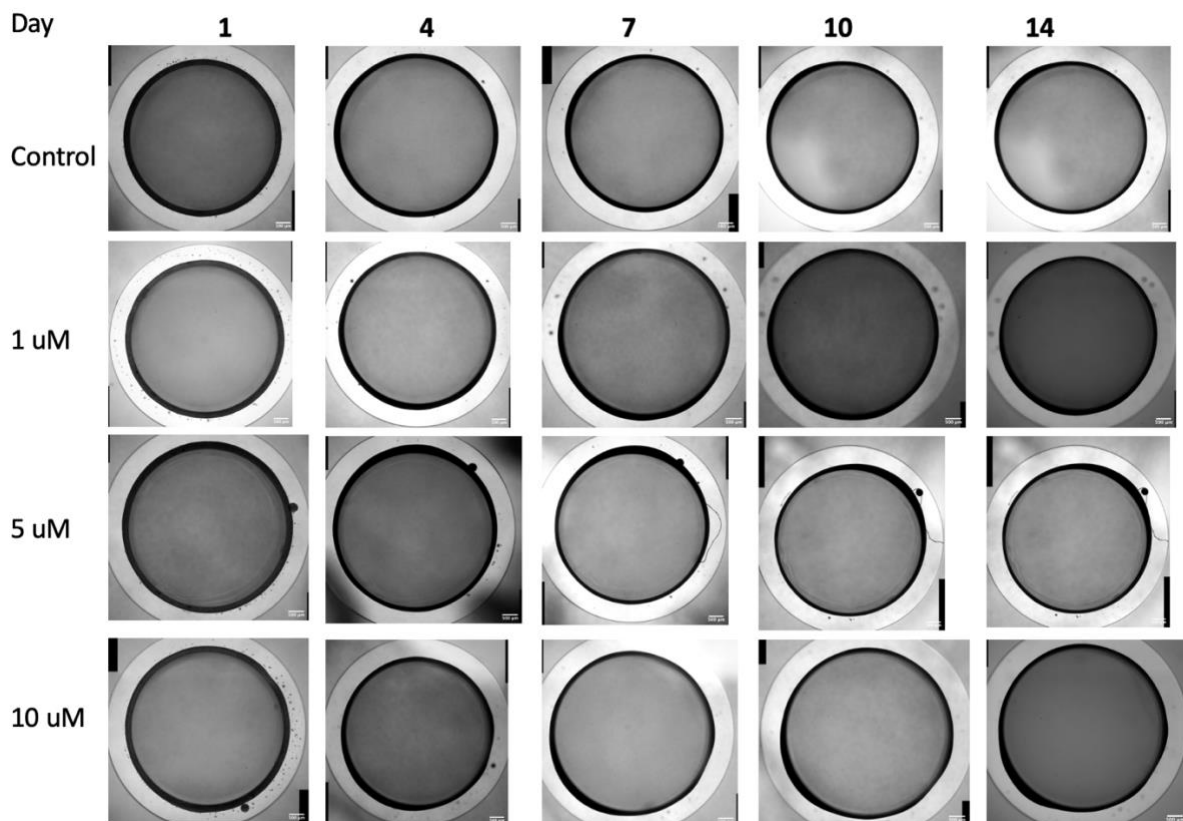


Figure 6: The self-assembled human dermal fibroblast constructed 3D microtissue rings around the peg. Twenty-four hours after seeding the jNHDF (Day 0) in 50:50 media, the rings were treated with 10 μM , 5 μM , 1 μM incyclinide, and 10 μM DMSO vehicle control, which was used to dissolve the incyclinide. Incyclinide is an inhibitor of MMP-2 by blocking the interaction of MMP-2 and MMP-14 to prevent activation. Two bright-field images of the top view on each ring were taken at 2x magnification on day 1, 4, 7, 10, and 14 and were stitched together by Fiji software scale bar is 500 μm .

Bright-field images of the top view on each ring were taken at 10X magnification on day 1, and 14 to visualize any changes to the surface of the ring (**Figure 7**). On Day 1, the control and incyclinide-treated groups with different doses exhibited smooth surfaces. On Day 14, compared with the control rings, the incyclinide-treated rings had a noticeable morphological change on their surface and more roughness was observed.

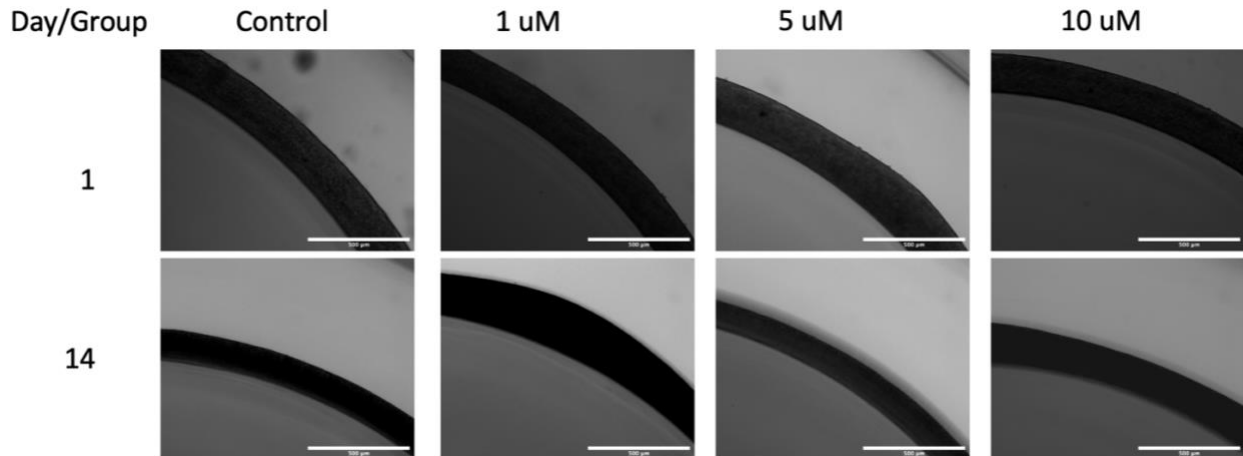


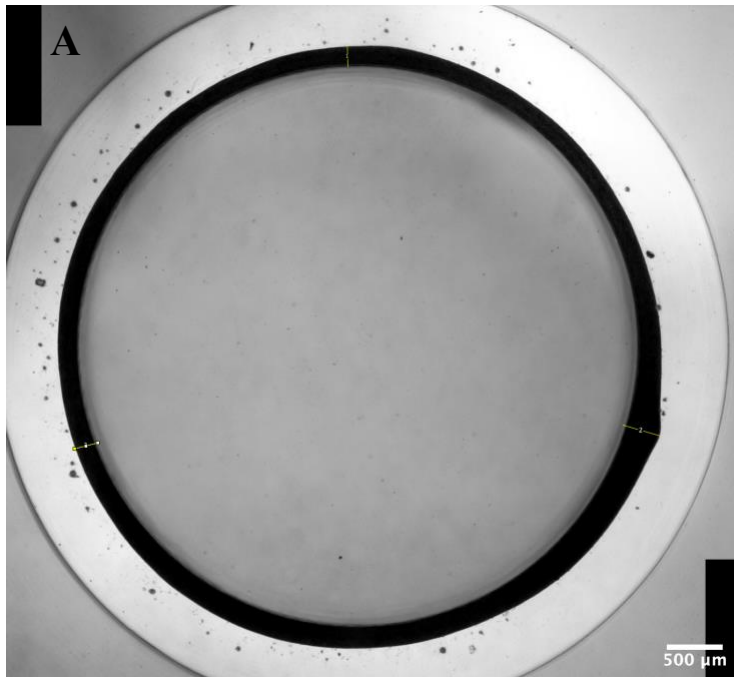
Figure 7: The morphological change of the incyclinide-treated rings. By comparing Day 1 with Day 14, the control rings did not exhibit differences in appearance and were smooth, while the 10 μM incyclinide-treated rings showed more roughness on their surface over time. All bright field images were taken at 10X magnification, and the scale bar is 500 μm .

Tissue ring thickness decreases over time in an incyclinide dose-dependent manner

The following objective was to compare the change in the thickness of the rings in the control group versus the 1, 5, 10 μM incyclinide-treated groups. Three measurements for each ring were taken and averaged for analysis (**Figure 8A**). In all groups, including control and drug-treated groups, the thickness of the rings decreased over time (**Figure 8B & 8C**). On Day 1, the mean thickness of the control group ($\mu = 258.5 \mu\text{m}$) was very close to the mean thickness of the 1 μM , 5 μM , and 10 μM incyclinide-treated groups ($\mu = 229.6, 242.1, 233.8 \mu\text{m}$), and there was no significant difference between the control and drug-treated groups. All measurements in each group were supposed to be similar on Day 1 since there was no drug treatment from Day 0 to Day 1, and the bright field images were taken before the drug was added.

Therefore, to minimize the initial difference in ring thickness among groups, the results from all measurements, including the values on Days 4, 7, 10, and 14, were normalized to the average thickness in each group on Day 1. Two-way ANOVA and Tukey's multiple comparisons test were used to calculate significant differences. As shown in Figure 3D, the initial value among all groups was around 100 (%). As the incyclinide dose increased from 0 to 1 μM , to 5 μM , and to 10 μM , the decline in microtissue ring thickness slowed over 14 days. From Day 7 to Day 14, the thickness of the control group was significantly lower than that of the incyclinide-treated group in general. On Day 4, the control group, the 1 μM , and the 5 μM groups had similar thicknesses, and all were slightly lower than the 10 μM drug-treated rings. On Day 7 and Day 10, the thickness of the rings in the vehicle control group (% = 90.3, 86.4) was significantly less than that of the 10 μM incyclinide treated rings (% = 95.6, 92.4). At the same time, there was no significant difference between the 1 μM , the 5 μM , and the control group, respectively. On Day 14, in addition to the

considerable difference between the control and 10 μM groups, there was a statistical difference between the vehicle control group (% = 77.5) and the 5 μM drug-treated group (% = 83.0). Surprisingly, the dose of incyclinide also affected the thickness of the rings. On Day 14, the thickness of the 1 μM incyclinide-treated group (% = 80.7) and the 5 μM group were significantly lower than that of the 10 μM group (% = 90.8). In general, over 14 days, the thickness of the control rings continuously decreased at the fastest rate, and next was the 1 μM group, followed by the 5 μM group. Eventually, the 10 μM incyclinide-treated rings declined with the slowest trend. The 10 μM drug-treated group decreased from Day 1 to 7 and then maintained a similar size from Day 7 to Day 14. This could be due to the changes in ECM content caused by the incyclinide, which inhibited MMP-2.



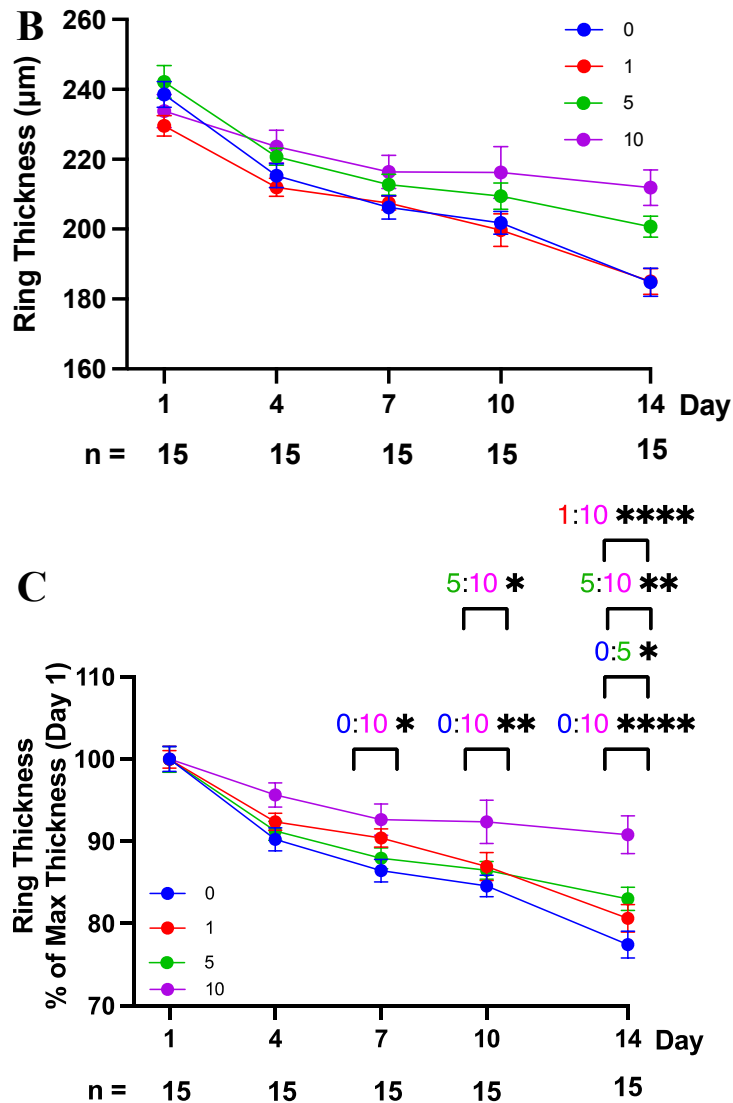


Figure 8: Incyclinide affects the thickness of 3D microtissues of dermal fibroblast rings in a dose-dependent manner. (A) Three measurements were taken and averaged for each ring. (B) The average thickness of each time point was calculated and connected to the graph. Overall, the thickness of the ring decreased over 14 days among all groups. (C) Data were normalized to the starting thickness on Day 1 in each group for better comparisons. On Day 1, all measurements were normalized to 100. On Day 14, the ring thickness between the vehicle control group and the 5 µM group, as well as the control and the 10 µM drug-treated group, exhibited statistically significant differences. Meanwhile, the thickness in the 10 µM incyclinide-treated group was also statically higher than that in the 5 µM incyclinide-treated group. The vehicle control rings decreased fastest, while the highest inhibitor group decreased at the slowest rate. In between, the 1 and 5 µM experimental groups declined at a similar rate.

The dermal fibroblast rings migrate at different distances around the peg

The next step was to determine if incyclinide altered the upward migration of ring-shaped tissues. Tissue rings were treated with incyclinide starting at 24 hours after cell seeding, and side view images were obtained on Days 7 and 14. Each gel was removed from the plate without touching the tissue using a spatula and cut on one side with a razor blade. The cut gel was laid on its flat side, and a bright-field image was acquired. The upward migration of each tissue ring was measured as the distance from the bottom of the circular trough to the bottom of the tissue ring (**Figure 9A**). Three measurements for each ring were taken, and the average migrated distance was calculated from control untreated rings and the rings treated with incyclinide. The control tissue rings' upward migration versus incyclinide treated tissue rings was not significantly different ($p > 0.05$). Tissue rings in all groups migrated upwards at various distances, demonstrating the viability of the tissue rings.

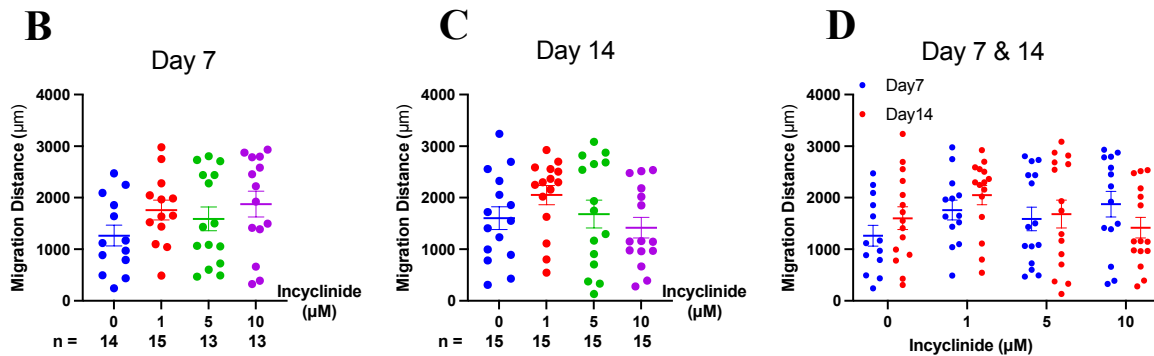
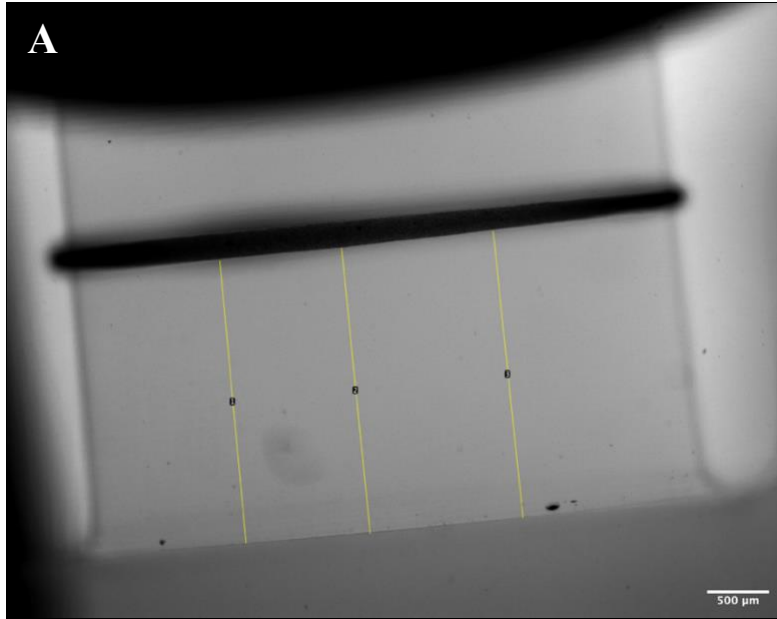


Figure 9: Microtissue rings migrated at different distances around the peg. (A) Each gel was cut on Day 14 to image the side length and the climbing distance of the rings. The migrated distance of the ring was the distance between the bottom of the well and the current height of the tissue. Three measurements of the distance migrated were taken from every mechanical-tested ring, one in the middle, one on the left, and the other on the right. (B) The average value of three measurements in all the rings in the control group and rings in the 1, 5, 10 μM incyclinide-treated groups were compared in the graph. There was no statistically significant difference in climbing distance between the control and incyclinide-treated groups on days 7 and 14.

Low doses of incyclinide do not affect the cross-sectional area or volume of rings

The next target was to quantify the cross-sectional area and volume difference among groups. Therefore, on Days 7 and 14, 4 - 5 rings from each group (0, 1 μ M, 5 μ M, 10 μ M) were selected to obtain the top view (**Figure 8A**) and side view (**Figure 10B**) bright-field images at 2x magnification. Three measurements for each ring were taken, and the average value of the top and side length in each ring was used to compute the cross-sectional area (A_0) and volume (**Figure 10A**). On Day 7, the cross-sectional area and volume of all groups were very close (**Figure 10C & 10F**). On Day 14, the top view thickness showed significant differences among the control, 5 μ M, and 10 μ M groups (**Figure 9**). The cross-sectional area and volume of the control group were significantly lower than those of the 10 μ M drug-treated group ($p = 0.019$, $p = 0.013$) (**Figure 10D & 10G**). Moreover, the cross-sectional area and the volume of the control, the 1 μ M, and the 5 μ M incyclinide-treated groups exhibited no significant difference ($P > 0.05$). This suggested that in control, 1 μ M, and 5 μ M groups, the difference in biomechanics was not caused by the difference in cross-sectional area. Interestingly, on Day 7 and Day 14, the volume and the A_0 mostly maintained similar levels among all groups.

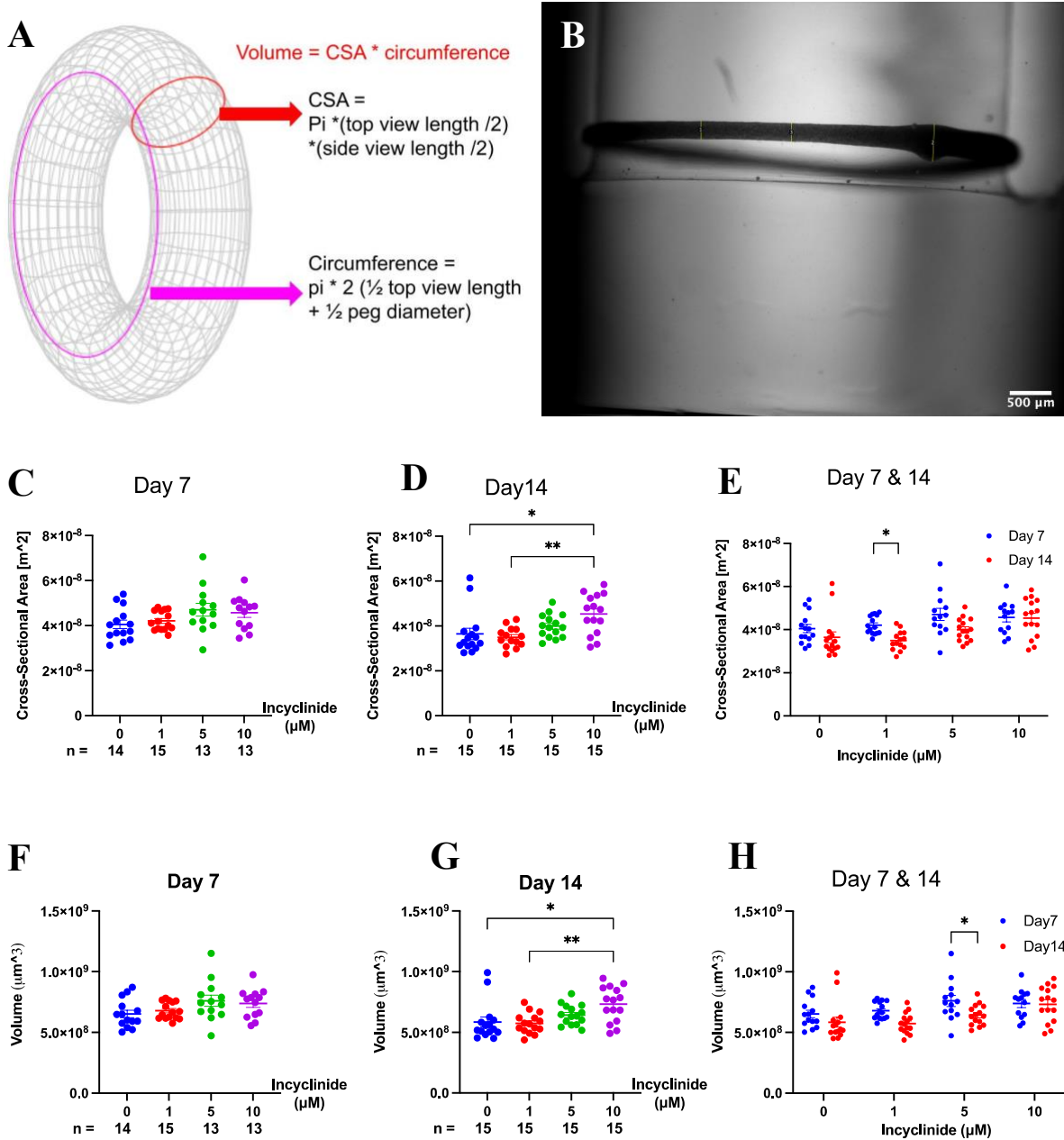
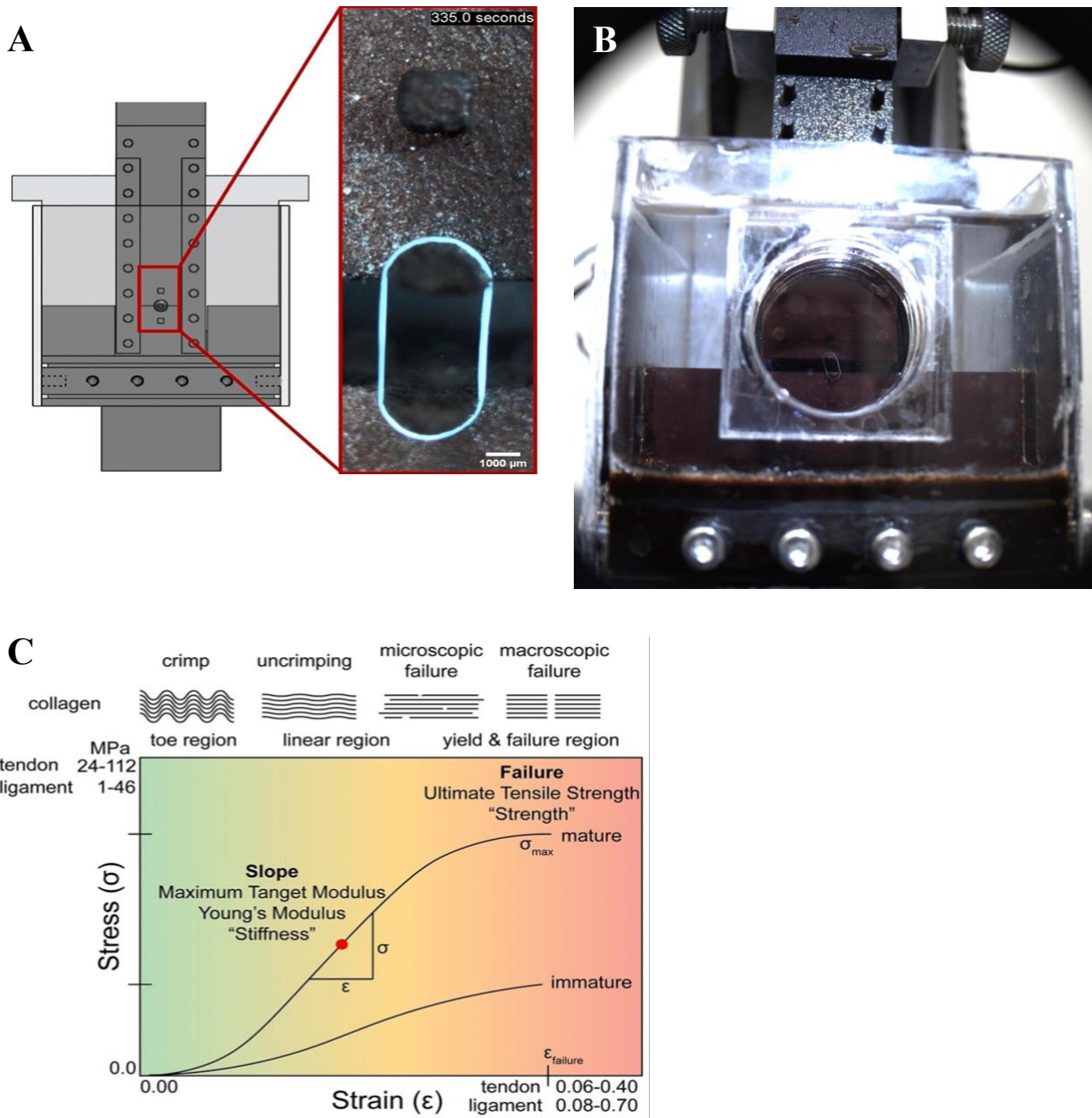


Figure 10: The cross-sectional area and the volume of the rings were calculated. The microtissue was formed in a shape like a toroid. (A) The graph shows the formula for calculating the cross-sectional area and the volume, which needs both measurements from the top and side view bright-field images of those rings [51]. The volume was calculated by the multiple of the cross-sectional area and circumference. (B) The side view of the rings was taken at a 2x magnification bright-field image, and the side lengths of the ring were measured at three diverse locations and were averaged for calculation. (C, D, F, G) At all time points, the vehicle control, the 1 μM , and 5 μM incyclinide treated groups showed no difference in both A_0 and volume. (D, G) There was an increase in volume and CSA in the group treated with the highest dose of incyclinide (10 μM) when comparing this group with the vehicle control and the low dose groups. (E, H) Across the timepoints, the A_0 and volume did not significantly differ in most of the groups.

Inhibition of MMP-2 increases the biomechanical properties of fibroblast tissue rings

MMP-2, an important drug target in cancer metastasis, plays a critical role in the breakdown of ECM during regular physiological circles, such as tissue repair, remodeling, and reproduction. The most crucial goal of this research was to investigate the effects of incyclinide, which acts as the inhibitor of MMP-2, on the tissue tensile strength and stiffness on Days 7 and 14. Five rings from each experimental group, including the 0, 1 μM , 5 μM , and 10 μM incyclinide-treated groups, were selected for mechanical testing for further research of the incyclinide on the tensile properties of the rings. To test the tensile strength of the rings, 3D printed customized grippers were embedded on an Instron tensile testing instrument with the lowest limited sensitivity of 5N loaded cell. An enclosure heater was used to keep the PBS at 37° C (**Video 1**). A .csv file was generated (including all the force applied to the tissue every second). The tissue was considered in tension, and the gauge length was recorded when the raw load was more significant than 5mN. Then, the cross-sectional area and the load-displacement curves from the file generated by the Instron were used to calculate the engineering stress-strain curve and true stress-strain curve. Those two curves were vital for quantifying the engineering ultimate tensile strength (UTS), engineering maximum tangent modulus (MTM), true UTS, and true MTM.



Video 1. Experimental setting of tensile testing on 3D microtissue rings. Benjamin Wilk designed the 3D printed customized Grippers embedded on an Instron 5943 with the lowest limited sensitivity of 5N loaded cell [37]. (A) An enclosure heater was used to keep the PBS at 37°C. The gripper consisted of two cuboid parts with a 1.5mm-radius half-cylinder. The rings were removed from the gel system and were positioned at a 5mm distance between two half customized grippers to archive quasi-static loading. Then, the load-displacement curves from the file generated by Instron. (C) With those curves, the engineering ultimate tensile strength, engineering maximum tangent modulus, true UTS, and true MTM were calculated by a custom python script [42]. Figure A & C was reprinted from Wilk et al. [37]

The engineering UTS is the maximum force applied on the microtissue ring during the mechanical testing before the breakage and is also shown as the highest point in the stress-strain curve (**Video 1C**). Engineering UTS is a critical point where the microtissue ring begins to break and weaken. The engineering MTM is the tissue stiffness of the dermal fibroblast tissue ring. In the tensile tests, the MTM was within the ‘linear region’ of the stress-strain curve which was generated by a python script. The slope of the curve was fitted by getting over eight percent of the linear fit on the curve [37]. Engineering UTS and MTM are only applicable to small deformation since these calculations assume the cross-sectional area and volume remain the same during the test, which rarely applies to most specimens in biology. True UTS and true MTM are calculated assuming that the tissue volume and cross-sectional area preservation occur. The tensile strength of the microtissue rings was determined by the decision of either the engineering or true stress-strain equations and the quantification of the location of the cross-sectional area.

From Day 7 to 14, the mechanical properties in the vehicle control group increased significantly as previously reported [37]. The engineering tissue strength and stiffness experienced a 2.07-fold and 2.08-fold increase from Day 7 to 14 ($p < 0.0001$). The significant increase in mechanical properties was potentially due to the change in collagen cross-linking [37].

On day 7, the mechanical properties among the 0, 1, and 5 μM incyclinide-treated groups exhibited no significant difference. The means engineering UTS in control, 1 and 5 μM were 2.70, 2.85, and 3.63 MPa respectively (**Figure 11A**). There were slight rises in all tissue strength and stiffness (**Figure 11 & 12**) as the dose of incyclinide increased, but there was no significant difference shown after the statistical tests. Therefore, at the early time point, the lower doses (1 and 5 μM) incyclinide effects on biomechanics were not evident.

On day 14, the mechanical properties between vehicle control and 1 μM incyclinide-treated rings presented no statistical difference, while these between vehicle control and 5 μM incyclinide group underwent a significant increase. On Day 14, as the rings got matured, compared to the control ($\sigma_{\text{max}} = 2.68 \text{ MPa}$, $\mu_{(\text{MTM})} = 17.45 \text{ MPa}$), the engineering strain and stiffness of the 1 μM group was slightly higher ($\sigma_{\text{max}} = 2.86 \text{ MPa}$, $\mu_{(\text{MTM})} = 18.1 \text{ MPa}$), but showed no statistical difference. However, the 5 μM experimental group ($\sigma_{\text{max}} = 3.63 \text{ MPa}$, $\mu_{(\text{MTM})} = 20.9 \text{ MPa}$) were statically higher ($p < 0.001$) than the control group (**Figure 11A-C, 12A-C**). Considering the influence of deformation during the tensile test, the true UTS and MTM increased significantly in the 5 μM drug-treated group ($\sim .37$ - and $\sim .26$ - fold increase compared to the vehicle control at Day 14 respectively) (**Figure 11D-F, 12D-F**). As mentioned previously, in the vehicle control group, 1 μM , and 5 μM incyclinide-treated group, the biomechanical change was not due to the change in the cross-sectional area since there was no statistical significance (**Figure 10**).

On Day 14, the tensile properties were significantly different between the 1 μM and 5 μM incyclinide-treated group. There was no significant difference in UTS between the control and 1 μM group despite the slight increase. At the same time, there was a substantial difference between the 1 μM ($\sigma_{\text{max}} = 3.86 \text{ MPa}$, $\mu_{(\text{MTM})} = 18.10 \text{ MPa}$) and 5 μM group ($\sigma_{\text{max}} = 3.63 \text{ MPa}$, $\mu_{(\text{MTM})} = 20.9 \text{ MPa}$) (**Figure 11C**).

The highest concentration of incyclinide (10 μM) resulted in tissues with the weakest strength and stiffness among groups on both day 7 and 14. On day 7, the engineering stiffness in 10 μM ($\mu_{(\text{MTM})} = 4.24 \text{ MPa}$) group were significantly lower than in 5 μM ($\mu_{(\text{MTM})} = 6.13 \text{ MPa}$) and 1 μM group ($\mu_{(\text{MTM})} = 5.72 \text{ MPa}$) (**Figure 11A**). On day 14, the tissue strength and stiffness in 10 μM incyclinide-treated group were statically lower than the control ($p < 0.0001$), 1 μM ($p < 0.0001$),

and 5 μM ($p < 0.0001$) (**Figure 11D**). This implied that 10 μM incyclinide might have toxicity effects on the fibroblast rings, which affected the biomechanics.

As mentioned previously on the dramatic increase of biomechanics in the control, a significant increment in biomechanics was also found in the 1 μM and 5 μM incyclinide-treated group. In the 1 μM drug-treated group, similar to the control group, the engineering UTS and MTM had a 2.07 and 2.16-fold growth across Day 7 to 14. Surprisingly, in the 5 μM group, the elevated rates in engineering strength and stiffness (~ 2.85 -fold and ~ 2.41 -fold) were greater than the control and 1 μM group (**Figure 11C & 12C**). This implied that there might be a correlation between the dose of incyclinide and the rate of tissue remodeling, including the formation of collagen-crosslinking.

Interestingly, from Day 7 to 14, the mechanical properties of rings treated with 10 μM incyclinide grew at the slowest rate. Across day 7 to 14, there was only a .80 to .92-fold increase in engineering UTS and MEM, whereas control rings increased in a 2.07 to 2.24-fold manner (**Figure 11C & 12C**). This implied that 10 μM incyclinide might have effects on the inhibition of cell growth.

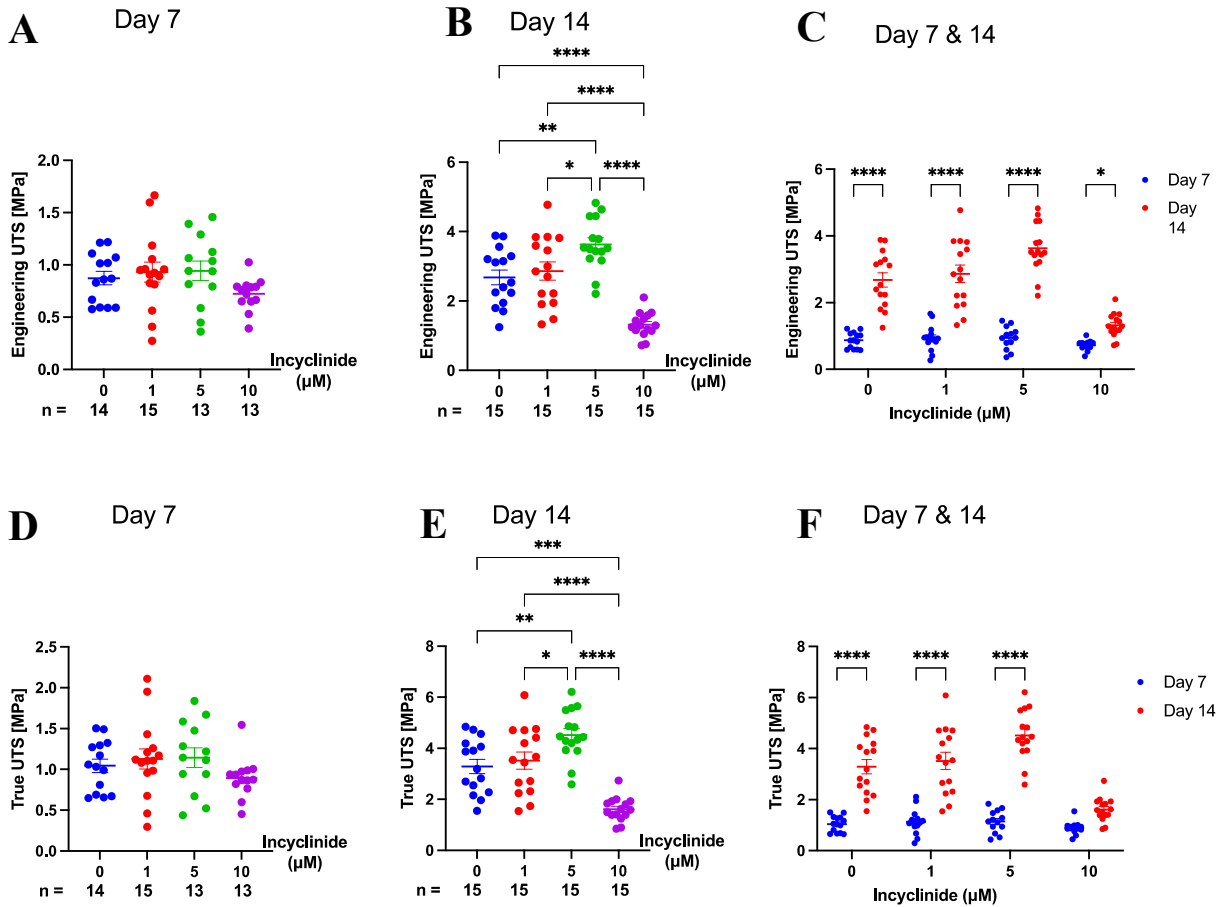


Figure 11: Incyclinide increased the tensile strength of rings at a dose of 5 μM . whereas a higher dose decreased tensile strength. The tensile strength was determined by the quantification of the cross-sectional area and the use of either engineering (A, B, C) or true stress and strain (D, E, F) formulas. Most of the research papers on mechanical properties made use of engineering stress and strain for direct comparison with other research studies. However, the engineering stress-strain curve did not consider the factors of tissue deformation, which the true stress-strain curve is quantified for. The comparison of tensile strength as different doses of incyclinide and time were determined by the engineering stress and strain versus the true stress and strain. (A, B, D, E) On Day 14, in comparison with the control group, at 5 μM , the tissue stress increased statistically significantly ($p < 0.0005$), while at 10 μM ($P < 0.05$), the UTS decreased. There was also a significant difference in UTS between the 1 and 5 μM drug-treated group ($P < 0.05$). (C, F) From day 7 to day 14, the UTS significantly increased among all groups ($P < 0.0001$), regardless of the highest incyclinide-treated group.

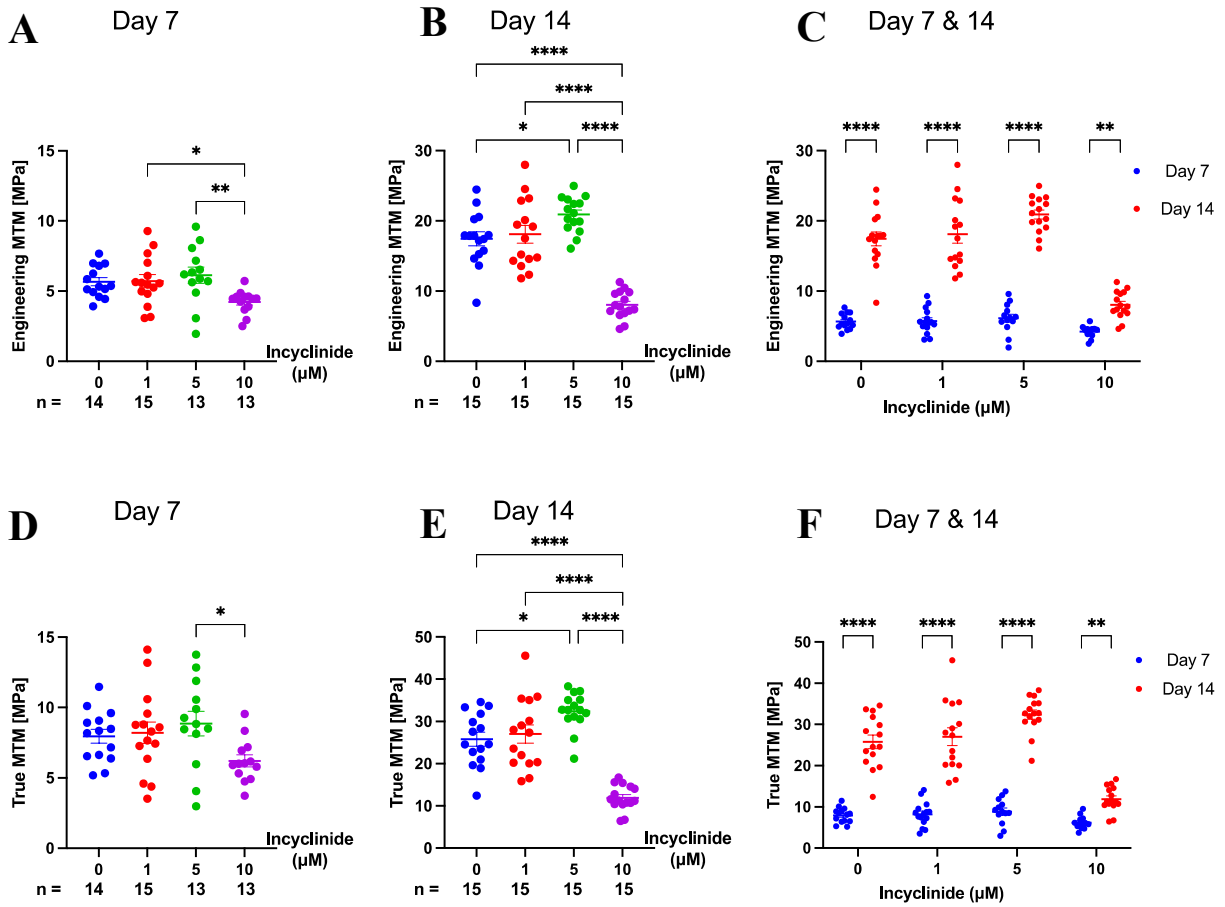


Figure 12: Incyclinide increased the stiffness at a dose of 5 μM, whereas a higher dose decreased stiffness. The stiffness of the fibroblast microtissue was decided by the quantification of the cross-sectional area and the use of either engineering (A, B, C) or true stress and strain (D, E, F) formulas. The engineering MTM and true MTM with different doses and time points were calculated by using the same dataset. (A, B, D, E) On day 14, compared with the vehicle control group, the tissue stiffness increased significantly at 5 μM ($p < 0.0005$), while at 10 μM ($P < 0.05$), the UTS decreased. (C, F) From Day 7 to 14, the MTM increased among all groups ($P < 0.001$).

Discussion and Conclusions

The MMPs are the vital enzymes to degrade various proteins in the ECM. Degradation of the ECM is significant for tissue development, morphogenesis, and remodeling [2]. MMP inhibitors have been studied and proposed as an emerging therapeutic target in cancer, osteoarthritis, fibrosis, and cardiovascular diseases. MMP-2 is produced by dermal fibroblast, and therefore, most likely is produced in our rings system [2]. Incyclinide, an effective MMP-2 inhibitor, was investigated in numerous research and evaluated in several clinical trials, including Phase II clinical trial for Kaposi sarcoma, Phase II clinical trial for recurrent brain tumors, and Phase I clinical trial of refractory metastatic cancer [31, 32, 33]. In this research, different doses of incyclinide (1 μM , 5 μM , and 10 μM), an inhibitor of MMP-2 were tested on fibroblast tissue rings. After seeding the jNHDF cells into the molds on Day 0, different concentrations of the incyclinide-treated medium were added on Day 1. The medium was changed on Days 2, 5, 7, 10, and 12. Bright-field images were obtained on Days 1, 4, 7, 10, and 14. On Days 7 and 14, top-view and side-view bright-field images of the rings were taken for the calculation of A_0 before mechanical testing. In our experiment, the testing got operated with an Instron tensile testing machine with customized grippers. The extension length and the raw load were recorded when the raw force exceeded 5mN. The UTS and MTM were then calculated by the Python script developed by Wilks *et. al.* [37] The strength and stiffness of the tissue rings were determined using the engineering or true stress and strain equation and the quantification of A_0 . In this research, the A_0 in control, 1 μM , and 5 μM groups showed no significant differences. Therefore, the difference in biomechanics was not caused by the difference in A_0 . Incyclinide inhibits the MMP-2 by inhibiting the interaction between MMP-2 and MMP-14, showing increases in the biomechanical properties at the dose of 5 μM .

Because MMP-2, produced by dermal fibroblast cells, can degrade the ECM. This research hypothesized that inhibition of MMP-2 will lead to an increase in ECM proteins and result in stronger mechanical properties in the rings. This hypothesis was proven in this research but was dependent on the dose of incyclinide. We observed that the 5 μ M incyclinide-treated group exhibited stronger tissue strength and stiffness than those in the vehicle control rings on Day 14. Therefore, the dermal fibroblast rings did produce MMP-2. Moreover, the inhibition of MMP-2 led to more collagen and elastin in ECM and resulted in stronger biomechanics.

Interestingly, previous work has demonstrated that TGF- β and MMPs are involved in a complex regulatory loop in cancer invasion and fibrosis [20, 21, 42, 43, 51]. Finnon *et. al.* showed that there are two major TGF- β signaling pathways in the activation of gene expression, including the Smad2/3 pathway and the non-Smad2/3 pathway [50]. The non-Smad 2/3 pathway is involved in different pathways, including rho-associated protein kinase (ROCK). Wilks *et. al.* showed that a ROCK inhibitor had no impact on the biomechanics of the rings. However, Krstic *et. al.* showed that the Smad 2/3 pathway was most likely involved in the process of MMPs secretion [51]. According to Wilks *et. al.*, the addition of TGF- β 1 increased the biomechanics of the rings in a dose dependent manner. Conversely, when treated with SB-431542, an inhibitor of activin receptor-like kinase receptor (ALK) 4, 5, and 7, that blocks activation of TGF- β 1 and the Smad2/3 pathway, the biomechanics of the rings decreased [37]. TGF- β activated the secretion of Smad proteins and then modulated gene expression with various components, including transcription factor (TF), etc. This would result in an increase in the expression of MMP protein, including MMP-2. When latent MMP-2 is activated, it can activate TGF- β [50,51]. Wilks *et. al.* showed that TGF- β 1 leads to an increase in biomechanics. However, when we added 5 μ M incyclinide, an inhibitor of MMP-2, there was a rise in biomechanics. Therefore, it is reasonable to speculate that

in our ring system, the effect of MMP-2 on degrading collagen and other proteins of the ECM is more significant than MMP-2's effect when it activates TGF- β 1. Another explanation would be that there might be other factors in the system that activate the TGF- β 1, and lead to the increase in biomechanics in the rings.

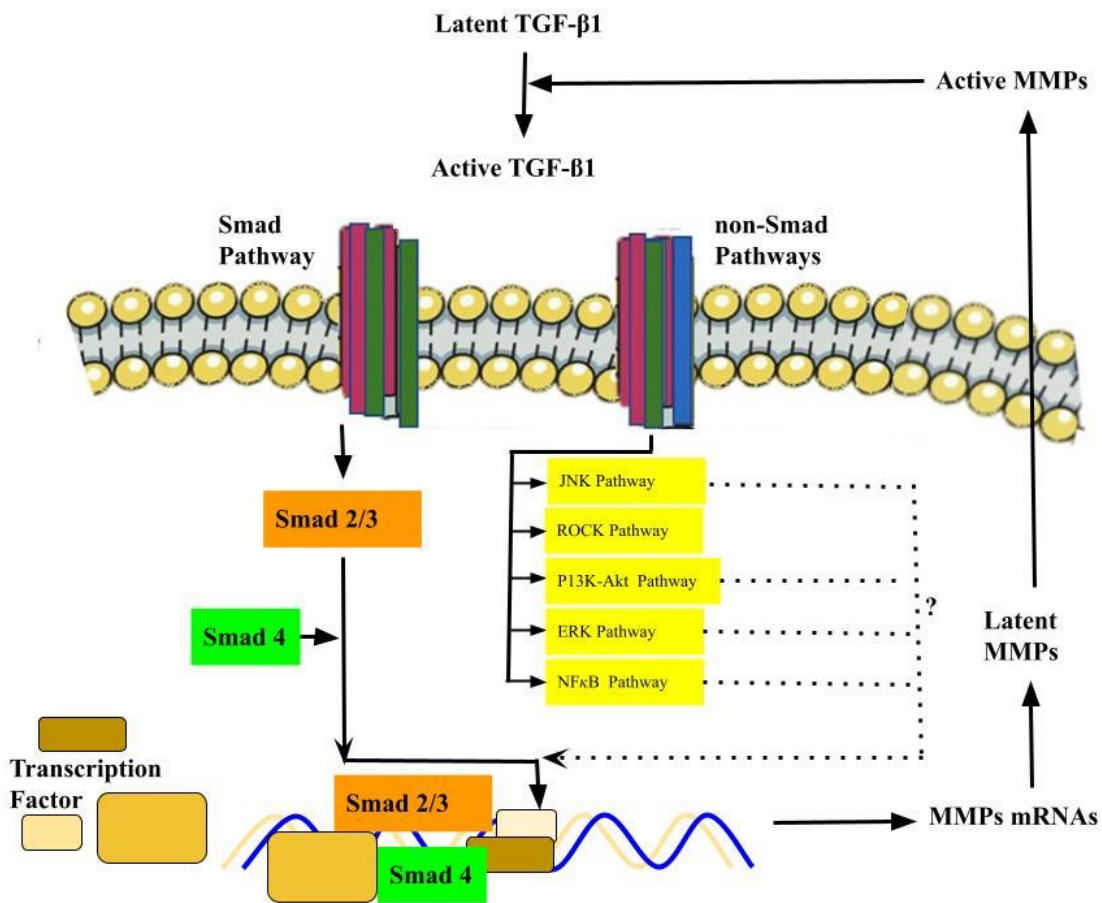


Figure 13: The schematic of the interaction of TGF- β and MMPs. There are two TGF- β signaling pathways: the Smad pathway and the non-Smad pathway. The Smad pathway produced Smad 2/3 proteins. The non-Smad pathway includes multiple parts, all of which can be activated by TGF- β . Together, the activation of Smad and potentially some non-Smad pathways promote the expression of MMPs. When latent MMPs are activated, and they can initiate the activation of TGF- β . Figure was reprinted from Krstic et al. and Finsson et al. [43, 51]

The biomechanics of the incyclinide-treated rings did not show an increase in a dose-dependent manner. According to Lokeshwar *et. al.*, when CaP139 cells, a prostate cancer cell line, were treated with incyclinide, MMP-2 enzymatic activity levels in the culture medium decreased by 35.0 %, and 56.7 %, with doses of 1 μM and 5 μM , respectively [27]. There was no significant difference in the mechanical properties of tissue rings between the control group and the 1 μM incyclinide-treated group, even though there was a significant increase in biomechanics between 1 μM and 5 μM groups on Day 14. This implies that 1 μM incyclinide was not a high enough dose to increase the mechanical properties of tissue rings. It is probably attributable to the difference between 2D and 3D cell culture systems and the differences in cell types.

In addition to inhibiting MMP-2, incyclinide is one of the most potent CMTs and has toxicity effects including the inhibition of cell growth, the inhibition of cell proliferation, and the apoptosis of cells [23]. Those effects could be the explanation for the significant decrease in biomechanics in the 10 μM incyclinide-treated group. According to Protasoni *et. al.*, the concentration of incyclinide that causes a 50 % growth inhibition of fibroblasts was 10.5 μM [23]. Protasoni *et. al.* also demonstrated that incyclinide stopped cell proliferation on Day 1 and started the cell apoptosis process on Day 5 when 8.1 μM of incyclinide was used applied to A549 cells, a cancer cell type in lung adenocarcinoma [23]. In that experiment, untreated A549 cells had logarithmic growth over 5 days [23]. In our research, the biomechanics of the 1 μM incyclinide-treated group were similar to the control group on Day 14, whereas the biomechanics of the 5 μM incyclinide-treated group were statically higher than the control group. However, as the concentration of incyclinide was increased to 10 μM , the biomechanics declined was statistically lower than the control as well as the 1 and 5 μM incyclinide-treated groups on Day 14. In addition to the decrease in biomechanics, the 10 μM incyclinide-treated group had a surface roughness on

Day 14 that was not present in the other groups. This could indicate that the high dose may be toxic or induces cell apoptosis. Therefore, as the incyclinide concentration approached 10 μ M, several toxicities, including the inhibitory effect on the dermal fibroblast cell growth and the effect on cell apoptosis, could have weakened the biomechanics of the rings.

In addition to the difference in mechanical properties among groups on Day 14, there was around a 2-fold increase in biomechanics in the vehicle control groups as rings matured from Day 7 to Day 14. This large increase in mechanics with the time of maturation was also observed in a previous study with fibroblast ring-shaped tissues [37]. The explanation for the significant increase from Day 7 to Day 14 is likely due to collagen crosslinking in the ECM during the maturation process [37]. Jones *et al.* demonstrated that an increase in stiffness was due to collagen crosslinking when they compared the data from lung tissue between healthy patients and patients with idiopathic pulmonary fibrosis (IPF) [46]. Also, an *in vivo* experiment showed that inhibition of the collagen cross-linking enzymes, lysyl oxidase like-2 (LOXL2) and LOXL3 leads to a decrease in tissue stiffness and an improvement in lung functions [46]. Other studies have shown that LOX inhibitors, including PXS-5153A, β -aminopropionitrile, and PAT-1251, can reduce collagen crosslinking in *in vitro* models [44, 45]. Interestingly, from Day 7 to Day 14, the increase in biomechanics (\sim 2.72-fold) in the 5 μ M incyclinide-treated group was slightly higher than the increase in the control group (\sim 2.13-fold). There was a 0.59-fold increase from control rings to the 5 μ M incyclinide-treated group. This might indicate that the inhibition of MMP-2 plays a role in affecting the rate of collagen crosslinking during the post-translational process.

Further experiments should include measuring the amount of collagen in the tissue rings after the mechanical testing to validate the statement that the inhibition of MMP-2 leads to more ECM proteins. It is also worth noting that, histology, with hematoxylin & eosin (H&E) and

Mason's trichrome (MT) staining, and multiphoton Second Harmonic Generation (SHG) imaging can be obtained from the fixed rings among all groups at Day 7 and Day 14. The H&E and the MT stains will allow for the visualization of the ECM composition, including the ratio of cells to ECM and cell alignment. The SHG will allow for the visualization of the collagen architecture, including collagen alignment and density. On Day 14, because of the increased biomechanics in the 5 μM groups, it is reasonable to hypothesize that the 5 μM incyclinide-treated rings have increased cell alignment and a higher collagen density than the vehicle control group. In Wilks *et al.*, the increase, and shift in the interfibrillar space correlated with the stronger mechanical properties of the rings [37]. Therefore, in the 5 μM incyclinide-treated groups, the SHG images should show better interfibrillar space in the collagen construct than those in the control group. Also, H&E staining could reveal cell death and cell apoptosis and determine the toxicity of incyclinide at 10 μM .

Another future experiment is the evaluation of the protein level of MMP-2 in cell culture supernatants by using the human MMP-2 ELISA kit (ab 267813) produced by Abcam [49] on the collected media on Day 7 and Day 14. Potentially, by combining the enzymatic level of MMP-2 and the mechanical data among groups, more information, such as the IC_{50} of incyclinide, could be generated in the system of 3D dermal fibroblast rings.

It is our long-term goal to test out treatments of incyclinide in more different doses, including 2.5 μM , 5 μM , and 7.5 μM , to further validate the effect of incyclinide dose on the mechanical properties of the 3D fibroblast rings. Furthermore, more efforts about the mechanism of action (MOA) of the relationship between TGF- β 1 and MMP-2 in the tissue rings would be interesting to test by comparing the mechanical properties and collagen content of the incyclinide-treated group, the TGF- β 1 treated group, and the combination of incyclinide and TGF- β 1 group. With the combination of incyclinide and TGF- β 1, it is reasonable to predict that those rings will

have stronger mechanical properties than the control and the simple treatment since there will be less expression of MMP proteins. Another experiment is very likely to be investigating the effect of the inhibitor of LOX on the tissue rings to test the hypothesis that the significant increase in the control group from Day 7 to Day 14 is due to collagen cross-linking. In summary, incyclinide can increase the biomechanics of the fibroblast tissue rings at 5 μ M as an inhibitor of MMP-2. However, more research and experiments are needed with 3D tissue rings to validate the dosage effects of incyclinide and the impacts on the cell and collagen content and alignment when MMP-2 is inhibited by incyclinide.

References

- [1] Frantz, C., Stewart, K. M., & Weaver, V. M. (2010). The extracellular matrix at a glance. *Journal of cell science*, 123(Pt 24), 4195–4200. <https://doi.org/10.1242/jcs.023820>
- [2] Laronha, H., & Caldeira, J. (2020). Structure and Function of Human Matrix Metalloproteinases. *Cells*, 9(5), 1076. <https://doi.org/10.3390/cells9051076>
- [3] Wang, X., & Khalil, R. A. (2018). Matrix Metalloproteinases, Vascular Remodeling, and Vascular Disease. *Advances in pharmacology (San Diego, Calif.)*, 81, 241–330. <https://doi.org/10.1016/bs.apha.2017.08.002>
- [4] Quiding-Järbrink, M., Smith, D. A., & Bancroft, G. J. (2001). Production of matrix metalloproteinases in response to mycobacterial infection. *Infection and immunity*, 69(9), 5661–5670. <https://doi.org/10.1128/IAI.69.9.5661-5670.2001>
- [5] Nagase, H., Visse, R., & Murphy, G. (2006). Structure and function of matrix metalloproteinases and TIMPs. *Cardiovascular research*, 69(3), 562–573. <https://doi.org/10.1016/j.cardiores.2005.12.002>
- [6] Mannello, F., & Medda, V. (2012). Nuclear localization of matrix metalloproteinases. *Progress in histochemistry and cytochemistry*, 47(1), 27–58. <https://doi.org/10.1016/j.proghi.2011.12.002>
- [7] Li, X., Jin, L., & Tan, Y. (2021). Different roles of matrix metalloproteinase 2 in osteolysis of skeletal dysplasia and bone metastasis (Review). *Molecular medicine reports*, 23(1), 70. <https://doi.org/10.3892/mmr.2020.11708>

- [8] Lindner, D., Zietsch, C., Becher, P. M., Schulze, K., Schultheiss, H. P., Tschöpe, C., & Westermann, D. (2012). Differential expression of matrix metalloproteases in human fibroblasts with different origins. *Biochemistry research international*, 2012, 875742. <https://doi.org/10.1155/2012/875742>
- [9] Wang, L., Luo, J., & He, S. (2007). Induction of MMP-9 release from human dermal fibroblasts by thrombin: involvement of JAK/STAT3 signaling pathway in MMP-9 release. *BMC cell biology*, 8, 14. <https://doi.org/10.1186/1471-2121-8-14>
- [10] Akagi, A., Tajima, S., Ishibashi, A., Yamaguchi, N., & Nagai, Y. (1999). Expression of type XVI collagen in human skin fibroblasts: enhanced expression in fibrotic skin diseases. *The Journal of investigative dermatology*, 113(2), 246–250. <https://doi.org/10.1046/j.1523-1747.1999.00663.x>
- [11] Martignetti, J. A., Aqeel, A. A., Sewairi, W. A., Boumah, C. E., Kambouris, M., Mayouf, S. A., Sheth, K. V., Eid, W. A., Dowling, O., Harris, J., Glucksman, M. J., Bahabri, S., Meyer, B. F., & Desnick, R. J. (2001). Mutation of the matrix metalloproteinase 2 gene (MMP2) causes a multicentric osteolysis and arthritis syndrome. *Nature genetics*, 28(3), 261–265. <https://doi.org/10.1038/90100>
- [12] Li, X., Jin, L., & Tan, Y. (2021). Different roles of matrix metalloproteinase 2 in osteolysis of skeletal dysplasia and bone metastasis (Review). *Molecular medicine reports*, 23(1), 70. <https://doi.org/10.3892/mmr.2020.11708>
- [13] Têtu, B., Brisson, J., Wang, C. S., Lapointe, H., Beaudry, G., Blanchette, C., & Trudel, D. (2006). The influence of MMP-14, TIMP-2 and MMP-2 expression on breast cancer prognosis. *Breast cancer research : BCR*, 8(3), R28. <https://doi.org/10.1186/bcr1503>

- [14] Tokuhara, C. K., Santesso, M. R., Oliveira, G., Ventura, T., Doyama, J. T., Zambuzzi, W. F., & Oliveira, R. C. (2019). Updating the role of matrix metalloproteinases in mineralized tissue and related diseases. *Journal of applied oral science : revista FOB*, 27, e20180596. <https://doi.org/10.1590/1678-7757-2018-0596>
- [15] Zhu, L., Xi, P. W., Li, X. X., Sun, X., Zhou, W. B., Xia, T. S., Shi, L., Hu, Y., Ding, Q., & Wei, J. F. (2019). The RNA binding protein RBMS3 inhibits the metastasis of breast cancer by regulating Twist1 expression. *Journal of experimental & clinical cancer research : CR*, 38(1), 105. <https://doi.org/10.1186/s13046-019-1111-5>
- [16] Merchant, N., Nagaraju, G. P., Rajitha, B., Lammata, S., Jella, K. K., Buchwald, Z. S., Lakka, S. S., & Ali, A. N. (2017). Matrix metalloproteinases: their functional role in lung cancer. *Carcinogenesis*, 38(8), 766–780. <https://doi.org/10.1093/carcin/bgx063>
- [17] Tauro, M., & Lynch, C. C. (2018). Cutting to the Chase: How Matrix Metalloproteinase-2 Activity Controls Breast-Cancer-to-Bone Metastasis. *Cancers*, 10(6), 185. <https://doi.org/10.3390/cancers10060185>
- [18] Gomes, L. R., Terra, L. F., Wailemann, R. A., Labriola, L., & Sogayar, M. C. (2012). TGF- β 1 modulates the homeostasis between MMPs and MMP inhibitors through p38 MAPK and ERK1/2 in highly invasive breast cancer cells. *BMC cancer*, 12, 26. <https://doi.org/10.1186/1471-2407-12-26>
- [19] Jezierska, A., & Motyl, T. (2009). Matrix metalloproteinase-2 involvement in breast cancer progression: a mini-review. *Medical science monitor : international medical journal of experimental and clinical research*, 15(2), RA32–RA40.
- [20] *Circle torus mathematics geometry topology, circle, sphere, shape, Rim Png*. PNGWing. (n.d.). Retrieved March 18, 2022, from <https://www.pngwing.com/en/free-png-xvish>

- [21] Waning, D. L., Mohammad, K. S., Reiken, S., Xie, W., Andersson, D. C., John, S., Chiechi, A., Wright, L. E., Umanskaya, A., Niewolna, M., Trivedi, T., Charkhzarrin, S., Khatiwada, P., Wronska, A., Haynes, A., Benassi, M. S., Witzmann, F. A., Zhen, G., Wang, X., Cao, X., ... Guise, T. A. (2015). Excess TGF- β mediates muscle weakness associated with bone metastases in mice. *Nature medicine*, *21*(11), 1262–1271. <https://doi.org/10.1038/nm.3961>
- [22] Golub, L. M., McNamara, T. F., D'Angelo, G., Greenwald, R. A., & Ramamurthy, N. S. (1987). A non-antibacterial chemically-modified tetracycline inhibits mammalian collagenase activity. *Journal of dental research*, *66*(8), 1310–1314. <https://doi.org/10.1177/00220345870660080401>
- [23] Protasoni, M., Kroon, A. M., & Taanman, J. W. (2018). Mitochondria as oncotarget: a comparison between the tetracycline analogs doxycycline and COL-3. *Oncotarget*, *9*(73), 33818–33831. <https://doi.org/10.18632/oncotarget.26107>
- [24] Incyclinide (CMT-3): MMP inhibitor: Medchemexpress. (n.d.). Retrieved March 30, 2022, from <https://www.medchemexpress.com/Incyclinide.html>
- [25] Golub, L. M., Ramamurthy, N., McNamara, T. F., Gomes, B., Wolff, M., Casino, A., Kapoor, A., Zambon, J., Ciancio, S., & Schneir, M. (1984). Tetracyclines inhibit tissue collagenase activity. A new mechanism in the treatment of periodontal disease. *Journal of periodontal research*, *19*(6), 651–655. <https://doi.org/10.1111/j.1600-0765.1984.tb01334.x>
- [26] Liu, Y., Ryan, M. E., Lee, H. M., Simon, S., Tortora, G., Lauzon, C., Leung, M. K., & Golub, L. M. (2002). A chemically modified tetracycline (CMT-3) is a new antifungal agent. *Antimicrobial agents and chemotherapy*, *46*(5), 1447–1454. <https://doi.org/10.1128/AAC.46.5.1447-1454.2002>

- [27] Lokeshwar, B. L., Selzer, M. G., Zhu, B. Q., Block, N. L., & Golub, L. M. (2002). Inhibition of cell proliferation, invasion, tumor growth and metastasis by an oral non-antimicrobial tetracycline analog (COL-3) in a metastatic prostate cancer model. *International journal of cancer*, 98(2), 297–309.
- [28] Bildt, M. M., Henneman, S., Maltha, J. C., Kuijpers-Jagtman, A. M., & Von den Hoff, J. W. (2007). CMT-3 inhibits orthodontic tooth displacement in the rat. *Archives of oral biology*, 52(6), 571–578. <https://doi.org/10.1016/j.archoralbio.2006.11.009>
- [29] Selzer, M. G., Zhu, B., Block, N. L., & Lokeshwar, B. L. (1999). CMT-3, a chemically modified tetracycline, inhibits bony metastases and delays the development of paraplegia in a rat model of prostate cancer. *Annals of the New York Academy of Sciences*, 878, 678–682. <https://doi.org/10.1111/j.1749-6632.1999.tb07760.x>
- [30] Cianfrocca, M., Cooley, T. P., Lee, J. Y., Rudek, M. A., Scadden, D. T., Ratner, L., Pluda, J. M., Figg, W. D., Krown, S. E., & Dezube, B. J. (2002). Matrix metalloproteinase inhibitor COL-3 in the treatment of AIDS-related Kaposi's sarcoma: a phase I AIDS malignancy consortium study. *Journal of clinical oncology : official journal of the American Society of Clinical Oncology*, 20(1), 153–159. <https://doi.org/10.1200/JCO.2002.20.1.153>
- [31] Dezube, B. J., Krown, S. E., Lee, J. Y., Bauer, K. S., & Aboulafia, D. M. (2006). Randomized phase II trial of matrix metalloproteinase inhibitor COL-3 in AIDS-related Kaposi's sarcoma: an AIDS Malignancy Consortium Study. *Journal of clinical oncology : official journal of the American Society of Clinical Oncology*, 24(9), 1389–1394. <https://doi.org/10.1200/JCO.2005.04.2614>

- [32] Rudek, M. A., New, P., Mikkelsen, T., Phuphanich, S., Alavi, J. B., Nabors, L. B., Piantadosi, S., Fisher, J. D., & Grossman, S. A. (2011). Phase I and pharmacokinetic study of COL-3 in patients with recurrent high-grade gliomas. *Journal of neuro-oncology*, *105*(2), 375–381. <https://doi.org/10.1007/s11060-011-0602-9>
- [33] Rudek, M. A., Figg, W. D., Dyer, V., Dahut, W., Turner, M. L., Steinberg, S. M., Liewehr, D. J., Kohler, D. R., Pluda, J. M., & Reed, E. (2001). Phase I clinical trial of oral COL-3, a matrix metalloproteinase inhibitor, in patients with refractory metastatic cancer. *Journal of clinical oncology : official journal of the American Society of Clinical Oncology*, *19*(2), 584–592. <https://doi.org/10.1200/JCO.2001.19.2.584>
- [34] Chu, Q. S., Forouzes, B., Syed, S., Mita, M., Schwartz, G., Cooper, J., Curtright, J., & Rowinsky, E. K. (2007). A phase II and pharmacological study of the matrix metalloproteinase inhibitor (MMPI) COL-3 in patients with advanced soft tissue sarcomas. *Investigational new drugs*, *25*(4), 359–367. <https://doi.org/10.1007/s10637-006-9031-6>

- [35] Rowinsky E, Eckhardt S, Rizzo J, Hammond L, Campbell E, Felton S, et al. Protracted daily treatment with Col-3, and oral tetracycline analog, matrix metalloproteinase (MMP) inhibitor, is feasible: a phase I pharmacokinetic and biological study [abstract]. *Proc ASCO* 2000;19:180.
- [36] Longo, U. G., Lamberti, A., Petrillo, S., Maffulli, N., & Denaro, V. (2012). Scaffolds in tendon tissue engineering. *Stem cells international*, 2012, 517165. <https://doi.org/10.1155/2012/517165>
- [37] Wilks, B. T., Evans, E. B., Howes, A., Hopkins, C. M., Nakhla, M. N., Williams, G., & Morgan, J. R. (2022). Quantifying Cell-Derived Changes in Collagen Synthesis, Alignment, and Mechanics in a 3D Connective Tissue Model. *Advanced science (Weinheim, Baden-Wuerttemberg, Germany)*, e2103939. Advance online publication. <https://doi.org/10.1002/advs.202103939>
- [38] Rhee S. (2009). Fibroblasts in three dimensional matrices: cell migration and matrix remodeling. *Experimental & molecular medicine*, 41(12), 858–865. <https://doi.org/10.3858/emm.2009.41.12.096>
- [39] Sensini, A., & Cristofolini, L. (2018). Biofabrication of Electrospun Scaffolds for the Regeneration of Tendons and Ligaments. *Materials (Basel, Switzerland)*, 11(10), 1963. <https://doi.org/10.3390/ma11101963>
- [40] Ristaniemi, A., Stenroth, L., Mikkonen, S., & Korhonen, R. K. (2018). Comparison of elastic, viscoelastic and failure tensile material properties of knee ligaments and patellar tendon. *Journal of biomechanics*, 79, 31–38. <https://doi.org/10.1016/j.jbiomech.2018.07.031>
- [41] Jin, Q., Li, T., Zhou, P., & Wang, Y. (2009, May 11). Mechanical researches on Young's modulus of scs nanostructures. <https://doi.org/10.1155/2009/319842>

- [42] Sensini, A., & Cristofolini, L. (2018). Biofabrication of Electrospun Scaffolds for the Regeneration of Tendons and Ligaments. *Materials (Basel, Switzerland)*, *11*(10), 1963. <https://doi.org/10.3390/ma11101963>
- [43] Philips, N., Keller, T., & Gonzalez, S. (2004). TGF beta-like regulation of matrix metalloproteinases by anti-transforming growth factor-beta, and anti-transforming growth factor-beta 1 antibodies in dermal fibroblasts: Implications for wound healing. *Wound repair and regeneration : official publication of the Wound Healing Society [and] the European Tissue Repair Society*, *12*(1), 53–59. <https://doi.org/10.1111/j.1067-1927.2004.012111.x>
- [44] Schilter, H., Findlay, A. D., Perryman, L., Yow, T. T., Moses, J., Zahoor, A., Turner, C. I., Deodhar, M., Foot, J. S., Zhou, W., Greco, A., Joshi, A., Rayner, B., Townsend, S., Buson, A., & Jarolimek, W. (2019). The lysyl oxidase like 2/3 enzymatic inhibitor, PXS-5153A, reduces crosslinks and ameliorates fibrosis. *Journal of cellular and molecular medicine*, *23*(3), 1759–1770. <https://doi.org/10.1111/jcmm.14074>
- [45] Cosgrove, D., Dufek, B., Meehan, D. T., Delimont, D., Hartnett, M., Samuelson, G., Gratton, M. A., Phillips, G., MacKenna, D. A., & Bain, G. (2018). Lysyl oxidase like-2 contributes to renal fibrosis in Col4 α 3/Alport mice. *Kidney international*, *94*(2), 303–314. <https://doi.org/10.1016/j.kint.2018.02.024>

- [46] ones, M. G., Andriotis, O. G., Roberts, J. J., Lunn, K., Tear, V. J., Cao, L., Ask, K., Smart, D. E., Bonfanti, A., Johnson, P., Alzetani, A., Conforti, F., Doherty, R., Lai, C. Y., Johnson, B., Bourdakos, K. N., Fletcher, S. V., Marshall, B. G., Jogai, S., Brereton, C. J., ... Davies, D. E. (2018). Nanoscale dysregulation of collagen structure-function disrupts mechano-homeostasis and mediates pulmonary fibrosis. *eLife*, *7*, e36354. <https://doi.org/10.7554/eLife.36354>
- [47] Adebayo, O., Hookway, T. A., Hu, J. Z., Billiar, K. L., & Rolle, M. W. (2013). Self-assembled smooth muscle cell tissue rings exhibit greater tensile strength than cell-seeded fibrin or collagen gel rings. *Journal of biomedical materials research. Part A*, *101*(2), 428–437. <https://doi.org/10.1002/jbm.a.34341>
- [48] Gwyther, T. A., Hu, J. Z., Christakis, A. G., Skorinko, J. K., Shaw, S. M., Billiar, K. L., & Rolle, M. W. (2011). Engineered vascular tissue fabricated from aggregated smooth muscle cells. *Cells, tissues, organs*, *194*(1), 13–24. <https://doi.org/10.1159/000322554>
- [49]“Human MMP2 Elisa Kit (AB267813).” *Abcam*, 24 Mar. 2022, <https://www.abcam.com/human-mmp2-elisa-kit-ab267813.html>.
- [50] Finnson, K. W., Almadani, Y., & Philip, A. (2020). Non-canonical (non-SMAD2/3) TGF- β signaling in fibrosis: Mechanisms and targets. *Seminars in cell & developmental biology*, *101*, 115–122. <https://doi.org/10.1016/j.semcdb.2019.11.013>
- [51] Krstic, J., & Santibanez, J. F. (2014). Transforming growth factor-beta and matrix metalloproteinases: functional interactions in tumor stroma-infiltrating myeloid cells. *TheScientificWorldJournal*, *2014*, 521754. <https://doi.org/10.1155/2014/521754>